Current Biology 23, 560–568, April 8, 2013 ©2013 Elsevier Ltd All rights reserved http://dx.doi.org/10.1016/j.cub.2013.02.047

Article

Electrophoresis of Cellular Membrane Components Creates the Directional Cue Guiding Keratocyte Galvanotaxis

Greg M. Allen,[1] Alex Mogilner,[3,4] and Julie A. Theriot[1,2,*]
[1]Department of Biochemistry
[2]Howard Hughes Medical Institute
Stanford University School of Medicine, Stanford, CA 94305, USA
[3]Department of Neurobiology, Physiology, and Behavior
[4]Department of Mathematics
University of California, Davis, CA 95616, USA

Summary

Background: Motile cells exposed to an external direct current electric field will reorient and migrate along the direction of the electric potential in a process known as galvanotaxis. The underlying physical mechanism that allows a cell to sense an electric field is unknown, although several plausible hypotheses have been proposed. In this work we evaluate the validity of each of these mechanisms.
Results: We find that the directional motile response of fish epidermal cells to the cathode in an electric field does not require extracellular sodium or potassium, is insensitive to membrane potential, and is also insensitive to perturbation of calcium, sodium, hydrogen, or chloride ion transport across the plasma membrane. Cells migrate in the direction of applied forces from laminar fluid flow, but reversal of electro-osmotic flow did not affect the galvanotactic response. Galvanotaxis fails when extracellular pH is below 6, suggesting that the effective charge of membrane components might be a crucial factor. Slowing the migration of membrane components with an increase in aqueous viscosity slows the kinetics of the galvanotactic response. In addition, inhibition of PI3K reverses the cell's response to the anode, suggesting the existence of multiple signaling pathways downstream of the galvanotactic signal.
Conclusions: Our results are most consistent with the hypothesis that electrophoretic redistribution of membrane components of the motile cell is the primary physical mechanism for motile cells to sense an electric field. This chemical polarization of the cellular membrane is then transduced by intracellular signaling pathways canonical to chemotaxis to dictate the cell's direction of travel.

Introduction

For over a century, it has been known that motile cells exposed to external information from an applied direct current electric field will migrate along the orientation of the electrical potential (galvanotax-electrotax) [1]. Cells respond to currents that are similar in magnitude to those that exist under normal physiological conditions, including during the development of embryos of some animals [2] and wound formation [3] due to a short-circuit of the trans-epithelial potential [4]. In addition, exogenous electric fields applied in vivo are sufficient to disrupt development [5] or produce directed migration [6]. At this time, the mechanisms that cells use to sense an external electrical field, transduce this signal to the cell migration apparatus, and then appropriately change the direction of migration remain controversial.

Galvanotactic behavior has been demonstrated thus far in over 30 metazoan-derived cell types, including neurons [7], lung cancer cells [8], and leukocytes [9], as well as in crawling single-celled organisms, including *Dictyostelium discoideum* [10] and many swimming (ciliated) protozoa [11]. It is far less common to see reports of animal cells that fail to galvanotax, and this usually correlates with poorly motile behavior [6]. Electric fields that produce galvanotaxis are typically in the range of 0.1 to 10 V/cm [3]. It has been established that galvanotaxis operates independently of sensing an external chemical gradient [12]; therefore, we can limit our discussion of a cellular sensor of an external electric field to the electrical dimensions of the cell.

These electrical properties of the cell are primarily dictated by the cell's plasma membrane. External to the plasma membrane, the cell adheres to a charged substrate and is bathed by a conductive ionic media. Due to the high resistance of the cellular plasma membrane compared to the external media and to the small size of the cell, most $(\gtrsim 99.999\%)$ of the current flow created by an external electric field will pass around the cell and will therefore have limited effect on intracellular components [13]. The shielding effect of the plasma membrane is bridged primarily by a set of membrane channels with selective permeability to ions. In addition, the plasma membrane itself is embedded with a large set of charged macromolecules and lipids, which will be directly acted on by an external electric field through Coulombic interactions. These extracellular charged components and the charged substrate will also induce electro-osmotic flow in the presence of an external electric field.

Given these physical constraints, we can limit our exploration of the galvanotactic sensing mechanism to the following set of four plausible physical hypotheses (Figure 1): (1) Cells will be asymmetrically excited due to hyperpolarization of the anodal side and depolarization of the cathodal side of the cell, changing the opening probability of voltage-gated ion channels and creating an asymmetric electromotive force for ionic flow once ion channels are open [10]. (2) Electro-osmotic flow created at the substrate will reorient cells through hydrodynamic shear as is seen with laminar fluid flow [14]. (3) Electrostatic and electro-osmotic forces at the plasma membrane will apply mechanical force on the cell or on tension-sensitive cell-surface components. (4) These same electrostatic and electro-osmotic forces at the plasma membrane will also redistribute the charged components of the membrane establishing a cathodal-anodal axis of polarity [15]. These nonexclusive mechanisms are summarized in Figure 1.

Each of these putative sensors of an external electric field would require signal transduction pathways to relay the directional information to the cytoskeletal players that produce cell migration. Most cell types respond to an electric field by migrating toward the cathode, although some (often similar) cell types respond by migrating to the anode [16, 17]. The

*Correspondence: theriot@stanford.edu

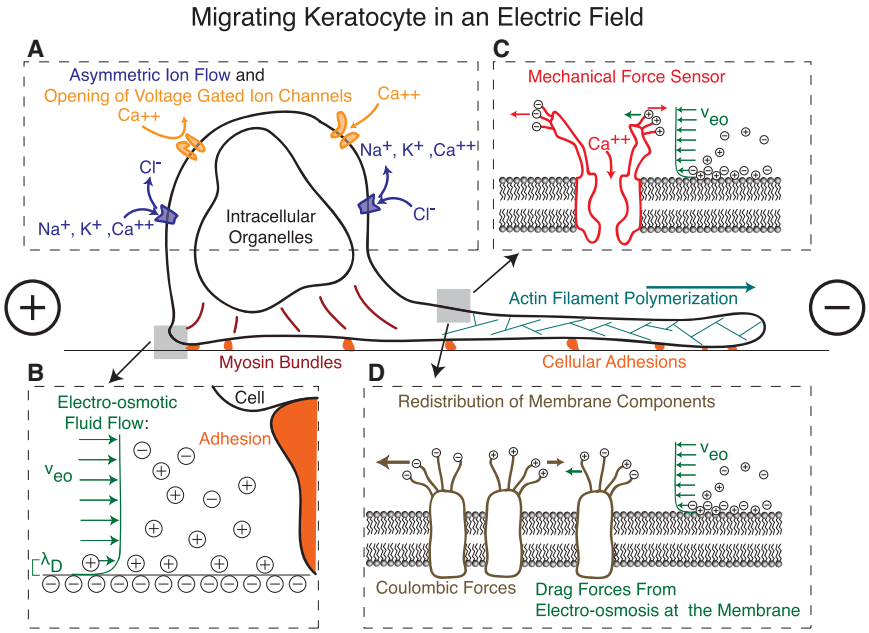

Figure 1. Models for Directional Sensing of a Keratocyte in an Electric Field

Visual description of the possible models for a galvanotactic response of a motile cell.

(A) An electric field will polarize the cell changing electromotive forces and opening/closing voltage-gated ion channels.

(B) Electro-osmotic flow, v_{eo}, at the charged migration surface will apply external force on the cell, which could for instance displace adhesions laterally.

(C) Electro-osmotic forces created by the relatively immobile charged ions in the cell membrane attracting a mobile double layer at the cell surface will combine with electrostatic forces on charged macromolecules and membrane components to produce mechanical work. As depicted, this could asymmetrically activate a force sensor creating a local signal that could be used to define the front and the back of the cell.

(D) Local electro-osmotic and electrostatic forces at the cell membrane will also electrophorese membrane components. Negatively charged components will move to the anode, and positively charged components will migrate to the cathode. Electro-osmotic forces at the membrane will also act to push proteins to one side of the cell or the other depending on the net surface charge of the cell.

mechanism underlying these antiparallel responses is unclear. Separate reports on the same cell type (human polymorphonuclear cells) have found opposing anodal versus cathodal galvanotactic responses [6, 18], which have been attributed to differences in extracellular calcium [19]. In addition, a mutant strain of *Dictyostelium* has been identified with a reversed (anodal) electrotactic response. This mutant phenotype could be replicated by inhibition of both cGMP and PI3K signaling activity [20], supporting the hypothesis that there is a separation between the physical mechanism of sensing an electric field and the eventual directional response.

Downstream of the unknown sensing mechanism, the current literature supports a hypothesis in which intracellular signaling pathways canonical to chemotaxis are used to transduce the galvanotactic signal. It is commonly noted that inhibition of PI3K disrupts the galvanotactic response of cells [21]. Galvanotaxis can also be blocked by inhibition of alternative signaling pathways, such as VEGF, ERK, and Rho/ROCK [16, 22]. In addition, cells in electric fields have asymmetric distributions of common polarity factors, including phosphatidylinositol (3,4,5)-trisphosphate (PIP3), PTEN, and growth factor receptors [9, 22, 23]. However, the signal transduction pathways of chemotaxis and galvanotaxis do not completely overlap because, unlike chemotaxis, PTEN inhibition improves the strength of a cell's galvanotactic response [9, 24], and in general the signaling pathways of galvanotaxis remain poorly understood.

The final step in the directional response to an electric field is the actual change in organization of the cytoskeleton of the motile cell to produce a change in direction. Little is known about the mechanical requirements for this process other than a described independence from the microtubule system and a general requirement for actin polymerization [25].

In this work, we seek to identify the cellular sensor of an external electric field by investigating the validity of each of the hypothetical physical mechanisms that could produce a galvanotactic response using the motile fish epithelial keratocyte model system. Keratocytes move at high speeds, with a simple shape, and, unlike cultures of mammalian cells, are robust to extreme physical perturbations, making them useful for understanding mechanical effectors of motility. In addition, keratocytes operate largely without requirements for external stimuli and are not known to be chemotactic. We find that the most likely sensing mechanism for galvanotaxis occurs due to electrophoretic redistribution of membrane components to the anode of the cell defining the rear. This polarity of membrane components is transduced by canonical intracellular signaling pathways that then dictate the cell's directionality.

Results

Keratocytes Migrate to the Cathode in an Electric Field

To examine the motion of spontaneously motile keratocytes, cells were imaged in sets of ~600 μm wide fields of view every minute for 1 hr. Cells under control conditions were equally likely to move in all directions (Figure 2A). Application of a 10 V/cm direct-current electric field biased the motion of motile cells toward the cathode (Figure 2B). Populations of cells exhibited a dose response in directional bias to applied potential, with a statistically significant response at 0.25 V/cm and a fully saturated response at 3 V/cm (Figure 2C).

For a given potential drop, decreasing the density of ions flowing over the cells by decreasing the salt concentration of the media decreased the effectiveness of the galvanotactic response despite a constant applied field strength (Figure 2C). We found that the strength of the galvanotactic response of cells in dilute and normal media collapsed to a single dose-response curve based on the dose of the ionic current density that flows over the cells (Figure 2D).

Electric fields have previously been claimed to provide a kinetic cue, as well as a directional cue, with speed increasing with increasing applied voltage [23, 26]. Similarly, under our standard conditions for inducing galvanotaxis within a

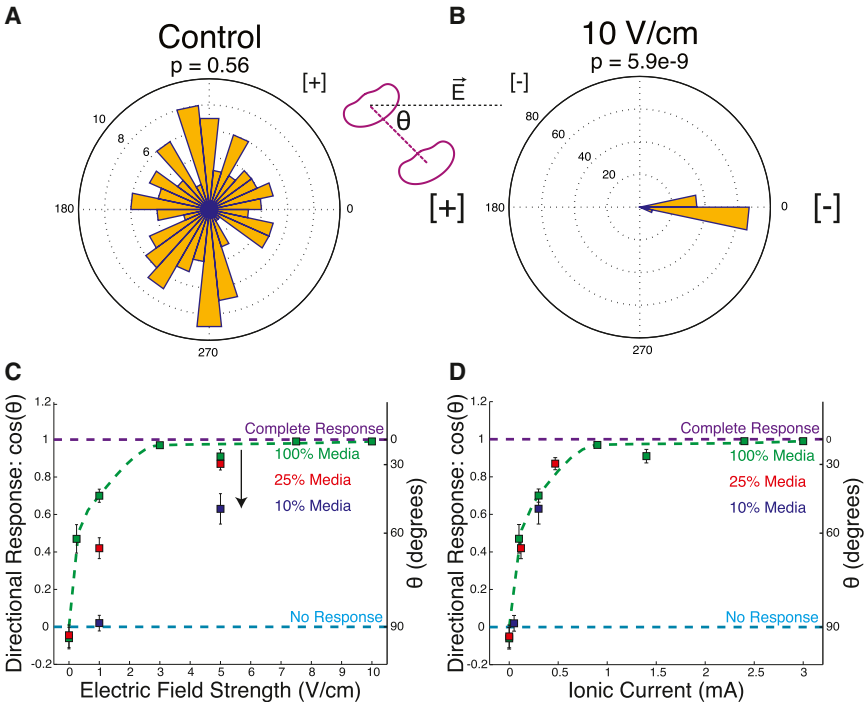

Figure 2. Keratocytes Migrate to the Cathode in an Electric Field

(A and B) Rose plots of the distribution of angles traveled in populations of 137 control cells (p = 0.56; A) and 110 cells in an electric field of 10 V/cm ($p = 5.9 \times 10^{-9}$; B), with the cathode oriented toward the right. The p value is calculated from a Kolmogorov-Smirnov test for a uniform distribution of angles traveled.

(C) The strength of the directional response is calculated for populations of cells as the mean ± SE of the cos(θ), where θ represents the direction that a cell travels relative to the electric field lines, as depicted graphically. A cos(θ) of 1 indicates a complete directional response toward the cathode (purple line), a cos(θ) of 0 indicates no response (cyan line), and a cos(θ) of −1 indicates a reversed response. Green points and fit line represent the dose response to the applied potential of cells in normal media. For a given applied potential, there was a decreased strength of response when media conductivity was decreased by mixing L-15 media 1:4 (red) or 1:10 (blue) with water.

(D) Replotting of the same data as in (C) in terms of current flow shows that for all salt concentrations the directional response is proportional to the ionic current. Given the constant flow cell geometry used in these analyses, current density, J, will depend on the measured current, I, and cross-sectional area of the flow cell, A, where $J = I/A = I/2\times10^{-7}m^2$.

See also Figures S1, S6, and S7.

small-volume chamber, we found that keratocyte cell speeds increased with applied potential. However, a significant increase in temperature due to resistive heating was measured, which will independently increase cell speed [27] (Figure S1 available online). Thus in the robustly spontaneously motile keratocytes, there is no evidence of an electrokinetic effect, and as far as we can measure, we find that the electric field acts only to reorient existing cell motility machinery.

Disruption of Ionic Flux across the Cell Membrane Does Not Disrupt Galvanotaxis

Galvanotaxing cells in an external electric field will experience an estimated ~1% to 10% asymmetry in membrane voltage polarization, (Supplemental Discussion, section I), which in turn could produce asymmetries in ion flux through the plasma membrane and possibly provide a directional cue (Figure 1A). We examined this initial hypothesis by observing keratocyte migration in salt solutions without Na^+ (replaced with K^+ or Cs^+) or without K^+. Keratocyte migration remained intact under both salt conditions, and cells continued to migrate toward the cathode (Figure 3). Similarly, removal of extracellular calcium has been reported to not modify galvanotaxis in keratocytes and fibroblasts [14, 28].

Moreover, we found that the galvanotactic response of cells was insensitive to a Ca^{2+} ionophore and to an intracellular calcium chelator and buffering agent (10 μM A-23187 and 10 μM BAPTA-AM). Inhibitors for L-type Ca^{2+} channels (50 μM verapamil), the Na^+/H^+ exchanger NHE1 (20 μM amiloride), or the volume-regulated anion channel (50 μM DCPIB or 10 mM ATP or 10 mM ADP) again had no effect on the strength of cell's galvanotactic response (Figure 3).

These perturbations will not only disrupt typical chemical gradients that exist across the cell membrane, but will also modify the membrane potential of the whole cell. The opening probability of a typical voltage-gated ion channel depends on membrane potential over a range of ~20 to 60 mV. Therefore, replacement of Na^+ ions in the media with K^+ ions (expected depolarization, $\phi_M \gtrsim 0mV$) or addition of calcium ionophore (expected hyperpolarization, $\phi_M \lesssim -100mV$; [29]) should completely abrogate the ability of the channel to respond to a 5 mV change in potential from an external electric field. Nevertheless, these drastic perturbations had no effect on galvanotaxis.

In addition to asymmetric flux of electrolytes, an intracellular pH (pH_i) gradient could be produced by an external electric field [30] and guide the direction of migration [31]. However, using the membrane-permeable pH-sensitive dye BCECF, we found no detectable gradient of pH_i inside of either spontaneously motile cells or cells undergoing galvanotaxis (data not shown), and neither the H^+-ATPase inhibitor bafilomycin nor the H^+-ionophore dinitrophenol inhibited galvanotaxis (Figure 3).

Thus, after removal of any of the three most prevalent cations, repeated mechanistically distinct disruptions of the membrane potential that provides the electromotive driving force across the membrane, disruption of several sets of ion channels, and direct measurement of pH_i, we must conclude that there is no evidence to support the first hypothesis that asymmetries in ionic current through the plasma membrane drives the directional sensing of an electric field for a galvanotactic response.

Laminar Fluid Flow but Not Bulk Electro-osmotic Fluid Flow Can Direct Cell Motility

A second hypothetical cellular sensor of an electric field that has been suggested previously [14] would be a mechanical cellular response to the electro-osmotic fluid flow created at the charged surface that the cell migrates on (Figure 1B and

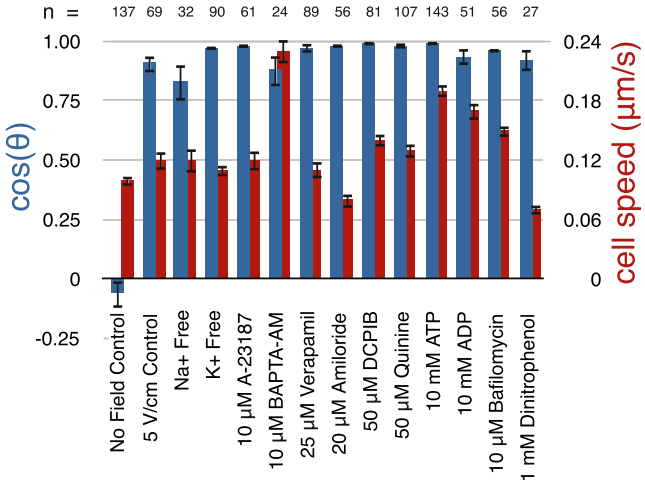

Figure 3. Ionic Flux Does Not Drive Galvanotaxis

Direction of travel of cells as quantified by the cos(θ) (blue) and mean cell speed (red) for populations of cells under specified perturbations, with n indicating the number of cells analyzed and error bars indicating the SEM. All perturbations were performed under an electric field of 5 V/cm (1.5 mA), except for the no-electric-field control cells. Perturbations include Na-free salt solution (Na^+ ions replaced with K^+ ions; similar results were seen with Cs^+ supplementation), K^+-free media (Na^+ supplemented), Ca^{2+} ionophore A-21387, intracellular Ca^{2+} chelator BAPTA-AM, L-type voltage-gated Ca^{2+} channel blocker verapamil, epithelial sodium channel (ENaC) and Na^+/H^+ exchanger (NHE-1) inhibitor amiloride, volume regulated anion channel (VRAC) inhibitors DCPIB and quinine, ATP and ADP (which can act as chloride channel inhibitors), vacuolar-type H-ATPase inhibitor bafilomycin, and proton ionophore dinitrophenol. See also Figure S7.

the Supplemental Discussion, section II). In support of this hypothesis, we found that cells exposed to fluid forces from laminar flow reorient and migrate in the direction of fluid flow at shear stresses of around 2.5 Pa and above (Figure S2, Movie S1, and Movie S2).

We then directly tested the role of electro-osmotic flow in reorienting cells in an electric field by reversing the direction of the electro-osmotic fluid flow. Under control conditions with negatively charged glass or tissue culture plastic as a substrate, electro-osmotic fluid flow at the surface was oriented toward the cathode with a magnitude of ~5 μm/s, (Figure 4A). After coating of the substrate with positively charge poly-L-lysine, the direction of flow was reversed toward the anode (Figure 4A). However, cells exposed to anodal electro-osmotic fluid flow did not modify their cathodal direction of motility or the sensitivity of the response (Figure 4B).

Since the force created by electro-osmotic flow on the cell is far smaller than that created by laminar shear stress (Supplemental Discussion, section II) and reversal of the direction of flow did not reverse the direction of galvanotaxis, we can conclude that our second hypothetical electric-field sensor (electro-osmotic fluid flow arising from the substrate) is not the driving physical mechanism behind galvanotaxis.

Galvanotaxis Is Sensitive to Changes in Extracellular pH

Because the plasma membrane electrically shields the interior of the cell and ionic flow through ion channels does not produce the galvanotactic response, the ionic current flowing over cells must control cell direction by affecting parts of the cell that extend outside of the plasma membrane. An electric field will have two primary effects on these exterior cellular components. All charged components will experience an electro-static force, whereas both charged and uncharged components will experience drag force from electro-osmotic fluid flow along the cell surface [28, 32], (Supplemental Discussion, section III).

To assess the importance of these forces to sensing an external electric field, we modified the strength and possibly direction of the applied forces by changing the charge of the extracellular membrane components by modifying extracellular pH. We found that keratocytes could survive and retain motility over a surprisingly broad pH range of 5.3 to 9.5 (Movie S3). However, the ability of cells to respond directionally to an electric field showed a dramatic dependence on pH (Figure 5A). From a complete galvanotactic response at a pH of 6.2 [cos(θ) = 0.82], there was no measured response of cells at a pH of 5.8 [cos(θ) = −0.12]. We can infer a direct effect of pH on the galvanotactic sensor because cell migration is otherwise stable (with stable cell speed), inhibition of galvanotaxis by an acidic pH was a reversible phenotype, and an acidic pH did not eliminate the ability of cells to respond directionally to shear stress (Figure S2). Of note, a pH of 6.0 has been previously identified in granulocytes as an isoelectric point in the switch between anodal migration in basic pH and cathodal migration in acidic pH [33].

Given that galvanotaxis fails critically as pH transitions from 6.2 to 5.8, the failure is most likely due to protonation. To distinguish the relative importance of electro-osmotic and electro-phoretic forces, the net charge of the cell at physiological pH of 7.4 was determined by measurement of the electrophoretic mobility of cells in suspension [34]. Unlike red blood cells, keratocytes were found to have a net positive surface charge at a pH of 7.4 (Figure 5B). Thus, we can rule out a significant effect of electro-osmotic flow, as the surface charge of the cell is positive with electro-osmotic flow oriented toward the anode, and further protonation would only increase the zeta potential at the membrane (ζ_m), increasing the strength of electro-osmotic flow to the anode. Instead, these data support a hypothesis in which an electric field applies force to a net negatively charged membrane component toward the anode, defining the rear of the cell.

The Kinetics of Galvanotaxis Are Dependent on Aqueous Viscosity

The electrophoretic force applied to a net negatively charged membrane component in an external electric field could act as a galvanotactic sensor either through direct mechanotransduction (Figure 1C) or by redistribution of components along the plasma membrane (Figure 1D). The force applied per molecule in an electric field of 1 V/cm would be quite small, requiring 62 elemental charges to generate 1 fN of force. There are few reports in the literature of stretch activated channels or mechanical transduction pathways responding to forces in this femtonewton range, with typical stimuli being 1 to 10 pN or higher [35]. We also found that inhibition of stretch activated calcium channels with 100 μM gadolinium had no impact on cellular galvanotaxis [cos(θ) = 0.91 at 5 V/cm]. However, it would only take 0.4 fN of force or 25 elemental charges to induce a significantly skewed protein distribution, plausible for highly glycosylated membrane proteins such as syndecans and stable oligomers (Supplemental Discussion, section IV).

To distinguish between these two hypotheses, we examined the kinetics of individual cell's directional response to

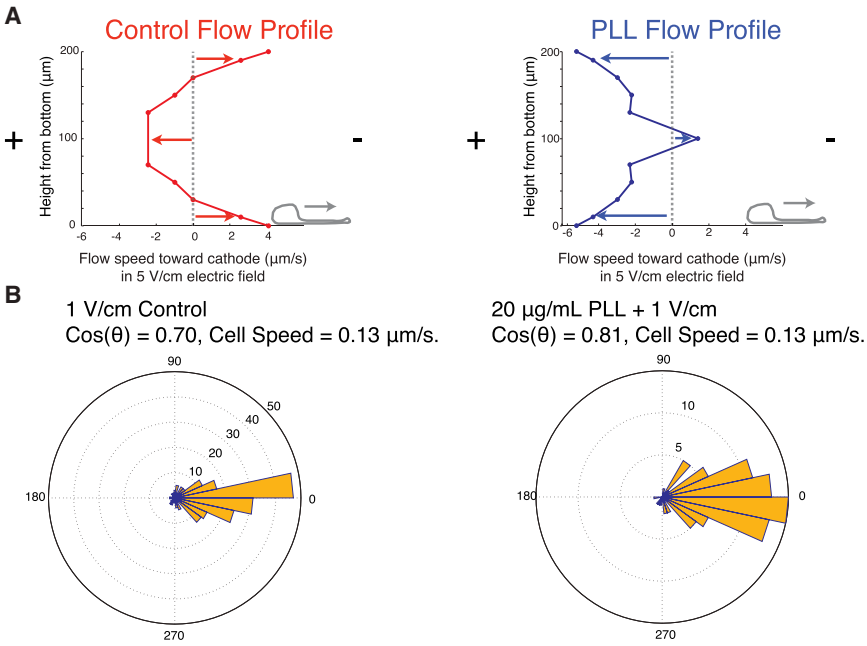

Figure 4. Keratocytes Migrate in the Direction of Applied Force, but Bulk Electro-osmotic Flow Does Not Drive Galvanotaxis

(A) Measured flow profile seen when a 5 V/cm electric field exists across the flow cell as measured by fluorescent tracer particles. Negligible particle motion is noted when the electric field is off. Recirculation flow in the center of the flow cell was noted due to the static head of pressure at the ends of the flow cell. Control conditions (left, red) produced flow toward the cathode. Coating of surfaces with 20 μg/ml poly-l-lysine (right, blue) reversed the direction of electro-osmotic flow to the anode. The cartoon keratocyte is not drawn to scale.

(B) Rose plot of directions of travel of keratocytes under an electric field of 1 V/cm (0.33 mA) with the cathode to the right under control conditions (left) and with the substrate patterned with 20 μg/ml poly-l-lysine (right). Cells exhibited a robust galvanotactic response to the cathode under both conditions.

See also Figures S2 and S7.

an electric field, which for redistribution of membrane components will depend on the electrophoretic mobility. Theoretically, we would predict that time required for the electrophoretic redistribution of charged membrane components and consequently the time for a cell to reorient in an electric field (*time to respond*) would both depend on the applied potential and the aqueous viscosity, while the time for a cell to lose directional orientation after an electric field is turned off (*time to forget*) would depend on the aqueous viscosity and the degree of previous polarization (Supplemental Discussion, section IV). We found that the *time to respond* was dependent on the strength of the applied potential (Figure 6). In addition, we found that increase of the aqueous viscosity from 1 to 50 cP with methylcellulose increased both the *time to respond* and the *time to forget*. Increase of aqueous viscosity had no effect on cell speed (95% of control) and no obvious visual perturbation of cell migration.

Confirming this result, we found that the time for a cell to switch directions in an electric field of 1 V/cm that was reversed had a weak but statistically significant positive correlation to cell size (Figure S3). These results are consistent with the hypothesis that electrophoretic motion of a membrane component to the anode/rear side of the cell dictates cell directionality. We directly visualized the redistribution of charged membrane components to the anode in an external electric field, with the fluorescently labeled lectin Concavalin A (ConA) (Figure S4). Redistribution to the anode in an electric field of 10 V/cm was observed over a time scale of 1 to 3 min, comparable to the time required for cells to begin to alter their direction.

Starting from our original four hypothetical mechanisms for a cell to sense an external electric field (asymmetric ionic polarization, shear stress from bulk electro-osmotic flow, activation of a mechanical force sensor, and electrophoretic membrane component redistribution), our data directly support only the final mechanism. This indicates that a cell senses an electric field by responding to the electrophoretic polarization of the components of its plasma membrane.

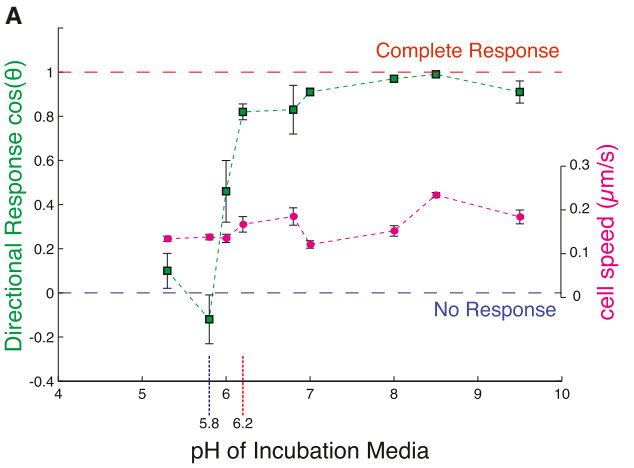

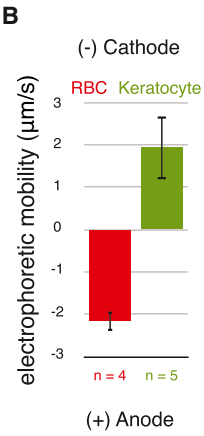

Figure 5. Keratocyte Galvanotaxis Is Sensitive to Protonation

(A) Measured cos(θ) (green) and cell speeds (magenta) ± SE for cells in media of variable pH when exposed to an electric field of 5 V/cm. Cells retained robust motility across this pH range. All measurements were done without the presence of serum, except at a pH of 5.8, 6.2, or 7.4. The presence of serum did not affect directionality at an acidic pH.

(B) The mean ± SE of the electrophoretic mobility of red blood cells and keratocytes in suspension and in an electric field of 1.5 V/cm. Red blood cells phoresed toward the anode, as would be expected from a negatively charged cell; keratocytes phoresed toward the cathode, as would be expected from a positively charged cell. Note the electrophoretic mobility speed is an order of magnitude larger than typical speeds of cell migration.

See also Figure S7 and Movie S3.

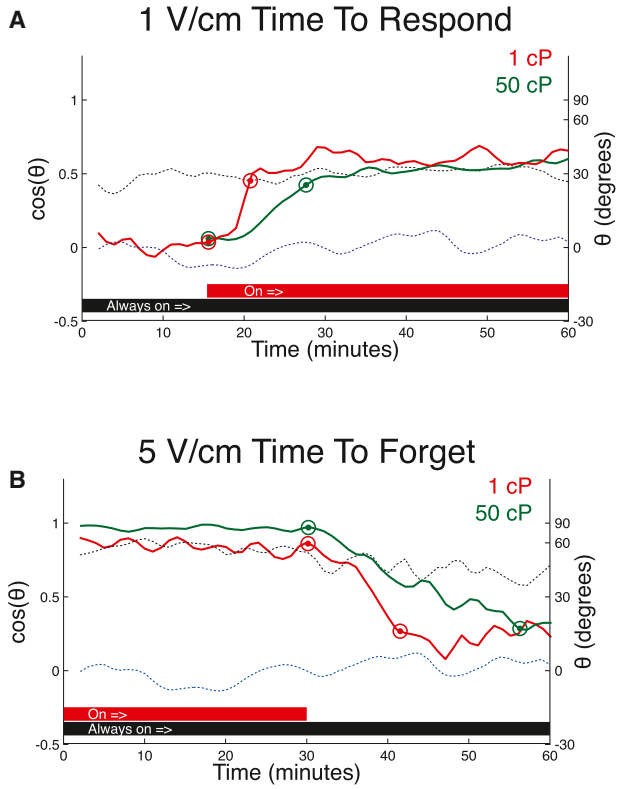

C

		Time to Respond (min)	n		Time to Forget (min)	n	
1 V/cm	1 cP	7.2 +/- 0.8	140	0.0019	12.6 +/- 0.7	136	0.0082
	50 cP	11.7 +/- 1.4	76		16.6 +/- 1.7	38	
5 V/cm	1 cP	4.1 +/- 0.3	145	0.0133	16.1 +/- 1.5	37	0.000008
	50 cP	5.2 +/- 0.4	57		26.5 +/- 1.7	31	

Figure 6. *Time to Respond* and *Time to Forget* Are Dependent on Aqueous Viscosity

The calculated mean[cos(θ)] is shown at every time point for all observed cells. Dashed black lines represent control cells at steady state in the electric field, dashed blue lines represent control cells at steady state without an electric field, red lines represent cells in 1 cP media, and green lines represent cells in 50 cP media + methyl-cellulose.

(A) Graphical depiction of the time of cells to respond to a 1 V/cm (0.3 mA) electric field, where the electric field is turned on at 15 min for cells in 1 and 50 cP media. We see cells in the lower-viscosity media reach steady-state behavior (red circle) faster than cells in higher-viscosity media (green circle).

(B) Graphical depiction of the time of cells to forget a 5 V/cm (1.5 mA) electric field, where the electric field is turned off at 30 min for cells in 1 and 50 cP. Again we see cells in the lower-viscosity media reach the new steady-state behavior (red circle) faster than cells in higher-viscosity media (green circle).

(C) The mean ± SE of the *time to respond* and *time to forget* were quantified from the time it takes each cell to reach steady state in minutes. The p value of unpaired Student's two-sample t tests between normal and elevated viscosity are marked in red for each.

See also Figures S3 and S4.

Downstream Signaling Pathways Are Required for Transduction of the Galvanotactic Signal

A model of electrophoretically induced polarization of membrane components holds a great deal of similarity to models of chemotaxis. Where chemotaxis involves a nonuniform chemical environment that is interpreted through a uniform set of membrane receptors [36], galvanotaxis appears to involve a uniform chemical environment that is interpreted through a nonuniform set of membrane components. The net effect is to create an internal chemical "compass" in a motile cell that is typically, although not exclusively, represented as an asymmetric accumulation of PIP3 at the leading edge [37]. However, in the spontaneously motile and nonchemotactic keratocyte, we found no requirement for extracellular serum factors (Figure S5), suggesting that the electrophoresed component is constitutively active. Therefore, to assess the identity of signal transduction pathways that define the internal compass, we investigated pharmacological inhibitors of known chemotaxis signaling pathways.

For keratocytes, we found that disruption of PIP3 production with the addition of PI3K inhibitor LY294002 greatly decreased the number of cells that were spontaneously motile, from 36% to 16%. Cells that retained motility moved at speeds that were ~75% those of controls. Inhibition of PI3K activity did eliminate the directional response of keratocytes at a field strength of 1 V/cm and produced a strikingly reversed response, toward the anode, in a field strength of 5 V/cm (Figure 7). At both field strengths, it does appear that the majority of cells are still oriented along the electric field lines; however, there is a dramatic increase in the number of cells with a reversed response, suggesting the existence of two competing signal transduction pathways downstream of the electrophoretic sensing mechanism.

We used further pharmacological perturbations to gain a glimpse into possible roles of other signaling pathways. We found that disruption of PKC signaling with 50 μM clomiphene or 10 μM tamoxifen inhibited the directional response in cells to an electric field [cos(θ) = –0.3 and 0.59, respectively]; however, inhibition of the Rho-associated serine/threonine kinase with 25 μM Y-27632 had no effect on galvanotaxis (Figure S5).

Cytoskeletal Reorganization Produced by Galvanotaxis Resembles Pathways Used in Spontaneous Migration

The final step in the directional response of a motile cell to an external electric field is the reorganization of the cytoskeleton to change the direction of travel. We therefore wished to determine whether galvanotaxis altered or merely reoriented the autonomous motility machinery.

At steady state, we found that cells imaged in an electric field did not have a dramatically different appearance than did cells imaged under control conditions (Figure S6 and Movie S5). When the direction of the field was alternated by reversal of the polarity of the two electrodes, cells would switch directions to migrate toward the new cathode over a 5 to 10 min time interval. Cells could change direction by either reversing their polarity (42% of events) or by smoothly turning in space (58% of events) (Figure S6). Cells that underwent a smooth turn in space developed asymmetries in shape that mirror those seen in keratocytes undergoing spontaneous turns in the absence of an electric field (G.M.A., unpublished data). In addition, similar to granulocytes [18], keratocytes were often noted to periodically overshoot a straight path toward the cathode, producing path oscillations (Movie S6).

We have found that inhibition of nonmuscle myosin II using the small-molecule inhibitor blebbistatin [38] did not affect the directional response of keratocytes [cos(θ) = 0.98 at 5 V/cm]. In addition, inhibition of adhesion maturation and signaling with the small-molecule inhibitors of focal adhesion kinase

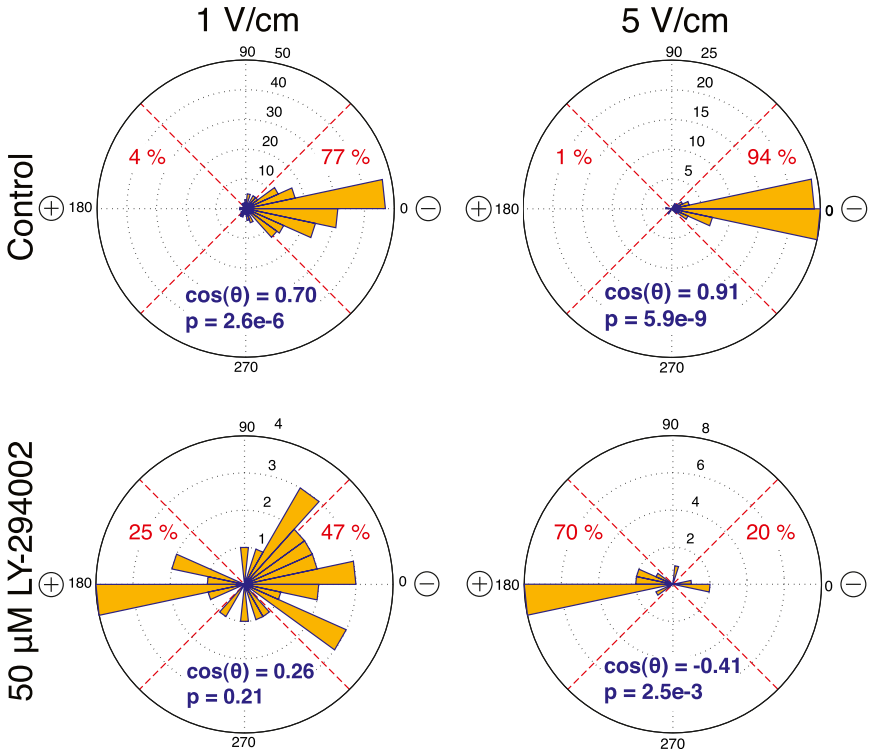

Figure 7. Keratocyte Galvanotaxis Is Sensitive to PI3K Activity

Rose plots of the distribution of angles traveled in populations of cells exposed to electric field of 1 and 5 V/cm (cathode oriented to the right) with and without the presence of PI3K inhibitor LY-294002. The fraction of cells traveling to the either the quartile of angles representing the cathode or anode are represented in red. Inhibition of PI3K causes some cells at 1 V/cm and a majority of cells at 5 V/cm to reverse direction to the anode. See also Figures S5 and S7.

FAK-14 [39] and PF-228 [40] similarly did not alter the ability of keratocytes to respond to an electric field [cos(θ) = 0.93 at 5 V/cm and cos(θ) = 0.87 at 1 V/cm, respectively]. Thus, the electric field appears to establish an internal compass that can use endogenous mechanical pathways to cause cell turning but does not have an absolute requirement for myosin contractility or for adhesion signaling and maturation.

Discussion

This work suggests that epithelial keratocytes reorient in an electric field due to redistribution of negatively charged membrane components to the anode, which is interpreted by intracellular signaling pathways commonly identified to play a role in chemotaxis to activate the same machinery that the cell uses for spontaneous turning. Redistribution of components of the cell's plasma membrane by an electric field has been experimentally demonstrated previously for ConA, low-density lipoprotein receptor, epithelial growth factor receptors, fibronectin receptor, and acetylcholine receptor [28, 32, 41, 42], lending plausibility to this proposed mechanism.

The membrane is composed of a complex set of charged proteins, lipids, and carbohydrates. For each charged membrane component exposed to an external electric field, there will be varying degrees of redistribution dependent on the relative charge of the macromolecule and the cell membrane. The identity of a single critical macromolecule for sensing an electric field is unknown. However, we can put likely constraints on the identity of this hypothetical sensor as a mobile complex with a large net negative charge (> ~ 25 e^-), a critical change in net charge around a pH of 6.0, and a role in determining the orientation of migration. One hypothetical sensor would be the transmembrane heparan sulfate proteoglycan, Syndecan-4, which is thought to interact with the cytoskeleton to promote migration [43], including through PKC-dependent pathways [44], and is found to be highly expressed in motile zebrafish keratocytes (S. Lou, personal communication).

Downstream of this polarity in membrane components, there is a clear role for intracellular signaling pathways, particularly in establishing cathodal versus anodal migration. In the work of Sun et al. [45] in keratocytes, the signal transduction pathway from the galvanotactic sensor to the machinery of cell motility is modeled as a strong PI3K-dependent pathway that defines the front at the cathode and a weak ROCK-dependent pathway that defines the back at the cathode. This is consistent with our data, in which without PI3K activity at sufficiently high field strengths, the secondary ROCK-dependent pathway is capable of defining the cell rear at the cathode and reorienting cells to the anode. We additionally identified that PKC is critical to both pathways, consistent with an established, though not definitive, promigratory role [46].

Consequent to activation of these intracellular signaling pathways, we found that cells can use the same mechanical mechanisms for changing the direction of migration as cells migrating outside of an electric field. This is the first evidence that downstream signaling pathways, canonical to chemotaxis, not only exist in the spontaneously motile and nonchemotactic keratocyte model system but also are able to act as an internal compass when provided with an external directional cue from an electric field.

Conclusions

The sensing mechanism for the galvanotaxis of motile keratocytes most consistent with our data is the global electrophoretic redistribution of one or several membrane components carrying a sufficiently large net charge to overcome thermal noise. Specifically, it appears that a negatively charged membrane component is electrophoresed to the cell rear to initiate cell reorientation. This physical separation of membrane components is then transduced by at least two competing intracellular signaling pathways, including one dependent on PI3K. These signaling pathways then influence the otherwise autonomously acting machinery of cell motility to change the direction of cell migration. Our data rule out directional sensing from electro-osmotic fluid flow and argue against asymmetric transmembrane potential acting as the galvanotaxis sensor.

Experimental Procedures

In brief, experiments were performed with cultures of Central American cichlid, *Hyposophys nicaraguensis*, keratocytes exposed to DC electric fields in thin flow cells in which single cell paths were measured by time-lapse phase-contrast microscopy. Fluid flow was measured by velocity of tracer particles, and cell electrophoretic mobility was measured by velocity of tracer cells in suspension. Oversight for protocols for working with animals was provided by APLAC review board. Temperature was measured by rhodamine intensity, pH_i by ratiometric dye BCECF, and the ConA distribution by Texas-red conjugated ConA. Full experimental details are provided in the Supplemental Experimental Procedures.

Supplemental Information

Supplemental Information includes Supplemental Discussion, seven figures, Supplemental Experimental Procedures, and six movies and can be found with this article online at http://dx.doi.org/10.1016/j.cub.2013.02.047.

Acknowledgments

We thank K.C. Huang, Alex Dunn, and Mark Tsuchida for discussion and Sara Bird for critical reading of this manuscript. This research was supported by the Howard Hughes Medical Institute, National Institutes of Health grant GM068952 to A.M., and the Stanford NIH Medical Scientist Training Program.

Received: August 7, 2012
Revised: January 28, 2013
Accepted: February 25, 2013
Published: March 28, 2013

References

1. Verworn, M. (1889). Die polare Erregung der Protisten durch den galvanischen strom. ("The polar excitation of protists by galvanic current"). Pflügers Archiv European Journal of Physiology *45*, 1–36.
2. Hotary, K.B., and Robinson, K.R. (1994). Endogenous electrical currents and voltage gradients in Xenopus embryos and the consequences of their disruption. Dev. Biol. *166*, 789–800.
3. McCaig, C.D., Song, B., and Rajnicek, A.M. (2009). Electrical dimensions in cell science. J. Cell Sci. *122*, 4267–4276.
4. Zhao, M. (2009). Electrical fields in wound healing-An overriding signal that directs cell migration. Semin. Cell Dev. Biol. *20*, 674–682.
5. McCaig, C.D., Rajnicek, A.M., Song, B., and Zhao, M. (2005). Controlling cell behavior electrically: current views and future potential. Physiol. Rev. *85*, 943–978.
6. Lin, F., Baldessari, F., Gyenge, C.C., Sato, T., Chambers, R.D., Santiago, J.G., and Butcher, E.C. (2008). Lymphocyte electrotaxis in vitro and in vivo. J. Immunol. *181*, 2465–2471.
7. Patel, N., and Poo, M.M. (1982). Orientation of neurite growth by extracellular electric fields. J. Neurosci. *2*, 483–496.
8. Yan, X., Han, J., Zhang, Z., Wang, J., Cheng, Q., Gao, K., Ni, Y., and Wang, Y. (2009). Lung cancer A549 cells migrate directionally in DC electric fields with polarized and activated EGFRs. Bioelectromagnetics *30*, 29–35.
9. Zhao, M., Song, B., Pu, J., Wada, T., Reid, B., Tai, G., Wang, F., Guo, A., Walczysko, P., Gu, Y., et al. (2006). Electrical signals control wound healing through phosphatidylinositol-3-OH kinase-gamma and PTEN. Nature *442*, 457–460.
10. Gao, R.-C., Zhang, X.-D., Sun, Y.-H., Kamimura, Y., Mogilner, A., Devreotes, P.N., and Zhao, M. (2011). Different roles of membrane potentials in electrotaxis and chemotaxis of dictyostelium cells. Eukaryot. Cell *10*, 1251–1256.
11. Jahn, T. (1961). Mechanism of ciliary movement. 1. Ciliary reversal and activation by electric current - Ludloff phenomenon in terms of core and volume conductors. J. Protozool. *8*, 369–380.
12. Nishimura, K.Y., Isseroff, R.R., and Nuccitelli, R. (1996). Human keratinocytes migrate to the negative pole in direct current electric fields comparable to those measured in mammalian wounds. J. Cell Sci. *109*, 199–207.
13. Mossop, B.J., Barr, R.C., Zaharoff, D.A., and Yuan, F. (2004). Electric fields within cells as a function of membrane resistivity—a model study. IEEE Trans. Nanobioscience *3*, 225–231.
14. Huang, L., Cormie, P., Messerli, M.A., and Robinson, K.R. (2009). The involvement of Ca2+ and integrins in directional responses of zebrafish keratocytes to electric fields. J. Cell. Physiol. *219*, 162–172.
15. Finkelstein, E.I., Chao, P.H., Hung, C.T., and Bulinski, J.C. (2007). Electric field-induced polarization of charged cell surface proteins does not determine the direction of galvanotaxis. Cell Motil. Cytoskeleton *64*, 833–846.
16. Zhao, M., Bai, H., Wang, E., Forrester, J.V., and McCaig, C.D. (2004). Electrical stimulation directly induces pre-angiogenic responses in vascular endothelial cells by signaling through VEGF receptors. J. Cell Sci. *117*, 397–405.
17. Li, X., and Kolega, J. (2002). Effects of direct current electric fields on cell migration and actin filament distribution in bovine vascular endothelial cells. J. Vasc. Res. *39*, 391–404.
18. Rapp, B., de Boisfleury-Chevance, A., and Gruler, H. (1988). Galvanotaxis of human granulocytes. Dose-response curve. Eur. Biophys. J. *16*, 313–319.
19. Franke, K., and Gruler, H. (1990). Galvanotaxis of human granulocytes: electric field jump studies. Eur. Biophys. J. *18*, 335–346.
20. Sato, M.J., Kuwayama, H., van Egmond, W.N., Takayama, A.L.K., Takagi, H., van Haastert, P.J.M., Yanagida, T., and Ueda, M. (2009). Switching direction in electric-signal-induced cell migration by cyclic guanosine monophosphate and phosphatidylinositol signaling. Proc. Natl. Acad. Sci. USA *106*, 6667–6672.
21. Arocena, M., Zhao, M., Collinson, J.M., and Song, B. (2010). A time-lapse and quantitative modelling analysis of neural stem cell motion in the absence of directional cues and in electric fields. J. Neurosci. Res. *88*, 3267–3274.
22. Zhao, M., Pu, J., Forrester, J.V., and McCaig, C.D. (2002). Membrane lipids, EGF receptors, and intracellular signals colocalize and are polarized in epithelial cells moving directionally in a physiological electric field. FASEB J. *16*, 857–859.
23. Meng, X., Arocena, M., Penninger, J., Gage, F.H., Zhao, M., and Song, B. (2011). PI3K mediated electrotaxis of embryonic and adult neural progenitor cells in the presence of growth factors. Exp. Neurol. *227*, 210–217.
24. Iijima, M., and Devreotes, P. (2002). Tumor suppressor PTEN mediates sensing of chemoattractant gradients. Cell *109*, 599–610.
25. Cooper, M.S., and Schliwa, M. (1985). Electrical and ionic controls of tissue cell locomotion in DC electric fields. J. Neurosci. Res. *13*, 223–244.
26. Finkelstein, E., Chang, W., Chao, P.-H.G., Gruber, D., Minden, A., Hung, C.T., and Bulinski, J.C. (2004). Roles of microtubules, cell polarity and adhesion in electric-field-mediated motility of 3T3 fibroblasts. J. Cell Sci. *117*, 1533–1545.
27. Ream, R.A., Theriot, J.A., and Somero, G.N. (2003). Influences of thermal acclimation and acute temperature change on the motility of epithelial wound-healing cells (keratocytes) of tropical, temperate and Antarctic fish. J. Exp. Biol. *206*, 4539–4551.
28. Brown, M.J., and Loew, L.M. (1994). Electric field-directed fibroblast locomotion involves cell surface molecular reorganization and is calcium independent. J. Cell Biol. *127*, 117–128.
29. Mitchell, M.R., and Martin, A.R. (1980). An electrophysiological study of the effects of ionophore A23187 on Nauphoeta salivary glands. Q. J. Exp. Physiol. Cogn. Med. Sci. *65*, 309–320.
30. Minc, N., and Chang, F. (2010). Electrical control of cell polarization in the fission yeast Schizosaccharomyces pombe. Curr. Biol. *20*, 710–716.
31. Martin, C., Pedersen, S.F., Schwab, A., and Stock, C. (2011). Intracellular pH gradients in migrating cells. Am. J. Physiol. Cell Physiol. *300*, C490–C495.
32. McLaughlin, S., and Poo, M.M. (1981). The role of electro-osmosis in the electric-field-induced movement of charged macromolecules on the surfaces of cells. Biophys. J. *34*, 85–93.
33. Fukushima, K., Sena, N., Innui, H., Tamai, Y., and Murakami, Y. (1953). Studies of galvanotaxis of leukocytes. Med. J. Osaka Univ. *4*, 195–208.
34. Lipman, K.M., Dodelson, R., and Hays, R.M. (1966). The surface charge of isolated toad bladder epithelial cells. Mobility, effect of pH and divalent ions. J. Gen. Physiol. *49*, 501–516.
35. Orr, A.W., Helmke, B.P., Blackman, B.R., and Schwartz, M.A. (2006). Mechanisms of mechanotransduction. Dev. Cell *10*, 11–20.
36. Swaney, K.F., Huang, C.-H., and Devreotes, P.N. (2010). Eukaryotic chemotaxis: a network of signaling pathways controls motility, directional sensing, and polarity. Annu. Rev. Biophys. *39*, 265–289.

37. Hoeller, O., and Kay, R.R. (2007). Chemotaxis in the absence of PIP3 gradients. Curr. Biol. *17*, 813–817.
38. Straight, A.F., Cheung, A., Limouze, J., Chen, I., Westwood, N.J., Sellers, J.R., and Mitchison, T.J. (2003). Dissecting temporal and spatial control of cytokinesis with a myosin II Inhibitor. Science *299*, 1743–1747.
39. Golubovskaya, V.M., Nyberg, C., Zheng, M., Kweh, F., Magis, A., Ostrov, D., and Cance, W.G. (2008). A small molecule inhibitor, 1,2,4,5-benzenetetraamine tetrahydrochloride, targeting the y397 site of focal adhesion kinase decreases tumor growth. J. Med. Chem. *51*, 7405–7416.
40. Slack-Davis, J.K., Martin, K.H., Tilghman, R.W., Iwanicki, M., Ung, E.J., Autry, C., Luzzio, M.J., Cooper, B., Kath, J.C., Roberts, W.G., and Parsons, J.T. (2007). Cellular characterization of a novel focal adhesion kinase inhibitor. J. Biol. Chem. *282*, 14845–14852.
41. Tank, D.W., Fredericks, W.J., Barak, L.S., and Webb, W.W. (1985). Electric field-induced redistribution and postfield relaxation of low density lipoprotein receptors on cultured human fibroblasts. J. Cell Biol. *101*, 148–157.
42. Zhao, M., Dick, A., Forrester, J.V., and McCaig, C.D. (1999). Electric field-directed cell motility involves up-regulated expression and asymmetric redistribution of the epidermal growth factor receptors and is enhanced by fibronectin and laminin. Mol. Biol. Cell *10*, 1259–1276.
43. Multhaupt, H.A.B., Yoneda, A., Whiteford, J.R., Oh, E.-S., Lee, W., and Couchman, J.R. (2009). Syndecan signaling: when, where and why? J. Physiol. Pharmacol. *60*(*Suppl 4*), 31–38.
44. Thodeti, C.K., Albrechtsen, R., Grauslund, M., Asmar, M., Larsson, C., Takada, Y., Mercurio, A.M., Couchman, J.R., and Wewer, U.M. (2003). ADAM12/syndecan-4 signaling promotes beta 1 integrin-dependent cell spreading through protein kinase Calpha and RhoA. J. Biol. Chem. *278*, 9576–9584.
45. Sun, Y., Do, H., Gao, J., Zhao, R., Zhao, M., and Mogilner, A. (2013). Keratocyte fragments and cells utilize competing pathways to move in opposite directions in an electric field. Curr. Biol. Published online March 28, 2013. http://dx.doi.org/10.1016/j.cub.2013.02.026.
46. Larsson, C. (2006). Protein kinase C and the regulation of the actin cytoskeleton. Cell. Signal. *18*, 276–284.

Current Biology, Volume *23*

Supplemental Information

Electrophoresis of Cellular Membrane Components Creates the Directional Cue Guiding Keratocyte Galvanotaxis

Greg M. Allen, Alex Mogilner, and Julie A. Theriot

Supplemental Discussion

I. Theoretical approximation of the effects of an external electric field on membrane polarity and ion flux

An applied external electric field, E_0, will create an induced electric potential, $\Delta\phi$, across the cell. The potential drop across the length of the cell will be dependent both on the cell radius, r, and the applied potential [1]

$$\Delta\phi = 1.5 \times E_0 \times r \tag{1}$$

A typical galvanotaxing cell is 5 to 10 μm in length and responds to electric fields in the range of 1 to 10 V/cm, which would create potential drops of 1 to 10 mV across the cell length. To put this into an appropriate context the resting potential of a cell, ϕ_M, is typically around -10 to -95 mV [2].

The electrical properties of the cell are primarily dictated by the cell's plasma membrane, which can be considered in part a selective resistor, with an estimated resistance in the tens of kilohm·cm^2 [3], and in part a capacitor, with an electric field across the membrane of around 100,000 V/cm [2]. Given the cell membrane's poor permeability to charge, most of the applied potential drop will be produced across the 5 nm thick bilayer perpendicular to the field [4]. For example, given a 10 μm spherical cell with a membrane resistance of 10,000 $\Omega \cdot cm^2$ in a 100 V/cm field, the electric field inside the cell has been estimated at 0.001 V/cm [5]. Therefore the external electric field will produce an electric field at the membrane of around 2,000 to 20,000 V/cm, which is about 10% of the characteristic inherent electric field.

This polarization at the cell membrane will be spatially inhomogeneous. If we consider the cell as a sphere in the external electric field, then the membrane potential at any point along the sphere, $\phi_M(\theta)$, can be approximated by [1]

$$\phi_M(\theta) = \phi_M - \Delta\phi \times cos(\theta) \tag{2}$$

where the anodal side of the cell will be hyperpolarized while the cathodal side of the cell will be depolarized with respect to the resting potential.

The magnitude of the polarization is dependent on both the strength of the external electric field and the length of the cell along the axis of the electric field. Thus, if anisotropic membrane polarization drives galvanotaxis, then the strength of the galvanotaxis response should depend on both the strength of the applied potential, as seen, and the size of the cell. However, a relationship between cell size and cathodal migration has not been identified in zebrafish or cichlid keratocytes [6, 7].

The main bridges between the external and internal electrical environments are ion channels. These ion channels permit current flow of around 1 to 10 pA/channel, allowing passage of 5,000 to 50,000 ions per millisecond; dependent on the electrical and chemical gradients across the membrane [8]. A subset of these ion channels are voltage-gated, where the open versus closed probability of the channel is a function of the membrane potential [9]. The estimated ∼1 to 10% asymmetric changes in the membrane potential in an external electric field would theoretically change the opening probability of these channels on the anodal versus cathodal side of the cell.

In addition, for all conducting ion channels an asymmetry in membrane polarity will create an asymmetry in ionic flux, as ions move down their electro-chemical gradient, due to relative de-polarization of the cathodal side and hyper-polarization of the anodal side of the cell in an external electric field [10]. This will produce a relative increase in the electro-motive driving force acting on cations on the anodal versus cathodal side of the cell, which could in principle polarize the cell motility apparatus.

II. Estimation of force applied on a cell by electro-osmotic and laminar fluid flow

Electro-osmotic fluid flow will arise from the substrate that cells migrate along, either the anionic proteoglycans of the extracellular matrix *in vivo* [11] or negatively charged glass *in vitro*. A given set of fixed charges will attract a diffuse double layer of opposing mobile charges in the ionic fluid through which cells migrate. The length scale of this double layer is described by the Debye length, κ^{-1}, essentially the distance at which ions in the bulk solution are electrically screened from the charge on the surface,

$$\kappa^{-1} = \sqrt{\frac{\varepsilon_r \varepsilon_0 k_B T}{2e^2 Z N}} \tag{3}$$

where ε_{r} is the dielectric constant, ε_0 is the permittivity of free space, k_B is the Boltzmann constant, e is the elemental unit of charge, T is absolute temperature, Z is the ionic strength and N is Avogadro's number.

When an external electric field is applied, this layer of mobile ions will be subject to Coulombic forces and will move to the appropriate electrode, dragging fluid with them and creating fluid flow. The velocity of electro-osmotic fluid flow, v_{eo}, for a given electrical potential, E, is set by the zeta potential of the surface, ζ_s, and the viscosity of the aqueous solution, η_{aq}, [12]

$$\frac{v_{eo}}{E_0} = \frac{-\varepsilon_r \varepsilon_0 \zeta_s}{\eta_{aq}} \tag{4}$$

Electro-osmotic flow reaches its maximal speed at the Debye length, approximately 8 $\mathring{A}$ for Leibovitz-15 media, and will maintain a plug flow into the bulk aqueous solution [13, 14].

To estimate the magnitude of the forces exerted by electro-osmotic flow, we optically measured the fluid velocity created by electro-osmotic fluid flow in our *in vitro* assay. At the focal plane of the substrate, fluid velocity was measured at $\sim$4 μm/s. Using an estimate of low Reynolds number Stokes drag force of electro-osmotic fluid flow, $F_{d,eo}$,

$$F_{d,eo} = 6\pi\eta_{aq} r(v_{eo} - v) \tag{5}$$

where r and v are the Stokes radius and the velocity of the cell, we can estimate the drag force applied to be in the range of 1 to 5 pN.

To estimate the viscous drag forces, F_d, created in laminar flow we can ignore the very thin lamellipodium and consider the motile keratocyte as a hemisphere with its flat side on the substrate surface, [15]

$$F_d = 13.5 \times \eta_{aq} \times Q \times R^2 \tag{6}$$

where Q is the gradient of the fluid velocity normal to the substrate surface and R is the height of the cell ($\sim$5 μm). For laminar flow in a chamber of height, $h = 200$ μm, the velocity at distance y from the surface V_y has the form:

$$V_y = V_0[hy - y^2] \tag{7}$$

Integration allows calculation of the average flow rate, $\bar{V}$,

$$\bar{V} = V_0 h^2/6 \tag{8}$$

With the velocity gradient near the chamber wall being defined,

$$Q = V_o h = 6\bar{V}/h \tag{9}$$

The flow rates of 4.9 to 8.3 mL/minute (shear stress of 2.5 to 4.2 Pa) that reoriented keratocytes would produce shear forces of 160 to 270 pN on the motile cell body. This value is two orders of magnitude less than the force reported to cause a cell to stall [16], but still might be significant enough to influence turning. This also suggests that the far smaller force on the cell created by electro-osmotic fluid flow is probably insufficient to guide the galvanotactic response.

It has previously been established that mechanical force applied locally with fluid flow from a micropipet to stationary keratocyte cytoplasts can induce symmetry breaking and initiate motility [17]. There are also numerous

reports of shear stress comparable to the magnitude that would be seen in blood vessels *in vivo* (∼1 to 5 Pa) [18] causing endothelial cells to reorient with their long axis parallel to the direction of fluid flow [19], and directing the migration of the single cell amoeboid *Dictyostelium discoideum* in the direction of fluid flow in a PI3K dependent process [20]. In contrast, we found that keratocytes do not require any of the components of the internal compass that play a role in galvanotaxis (PI3K, PKC), to migrate in the direction of applied force, suggesting a direct physical effect of the applied viscous drag forces (∼200 pN) on the mechanical systems that dictate cellular orientation.

The effect of laminar fluidic shear forces on a single protein of ∼10 nm in size would be at least an order of magnitude smaller than expected thermal fluctuations [21]; however, for a cell with a length scale of ∼10 μm a 20 pN/μm change in membrane tension would be created, which is a significant fraction of estimations of steady state membrane tension (100 pN/μm) [22]. Since the cell body will receive most of the applied fluidic force, this will create stretching of the cytoskeleton at the upstream side and compression at the downstream side, possibly providing a direct mechanical mechanism for cells to orient in the direction of an applied force. Alternatively, the force applied to the cell could be transduced to only a subset of the cellular adhesions that are upstream, such that the applied force on each adhesion will be in the low pN range, which is sufficient to cause known signaling and mechanical effects. At this point we can not distinguish between these hypotheses.

III. Electro-phoretic forces and electro-osmotic flow at the cell surface will apply force on external components of the plasma membrane

Most cells have a highly negatively charged surface with approximately 20×10^6 charges per cell ($\sim 5 \times 10^4$ charges per μm^2 [23]) and a protein density of ∼10,000 per μm^2 [24], which gives on average 5 net charges per membrane protein). These charges are relatively immobile when compared to soluble ions and will create a diffuse double layer locally. Therefore in an applied electric field, electro-osmotic flow will exist at the cell membrane dependent on net membrane charge [12].

In addition there will be an electro-static coulombic force, created by the external electric field on all charged components external to the plasma membrane, which will have a simple relationship between the force generated, F_e, the applied potential, E_0, and net charge of the force sensor, q_{net}, where $F_e = q_{net} \times E_0$.

As a rough estimate of the magnitude of these forces on galvanotaxing cells, we can consider the effect of electro-osmotic fluid flow on a relatively massive integrin-based focal adhesion. These adhesions bridge the cell membrane to the substrate over a distance of ∼30 nm [25]. A single focal adhesion complex has a measured size of ∼1 x 0.25 μm [26]. The magnitude of electro-osmotic flow will depend critically on the zeta potential of the surface and is difficult to measure. But, assuming a fluid velocity at the plasma membrane that is similar to the substrate, 5 μm/s, the corresponding drag force produced per focal adhesion complex would be ∼150 fN. Similarly it would take a net charge of a macromolecule in the thousands of elemental charges to achieve an applied coloumbic force of 150 fN. To put this value into context, the typical magnitude of force needed to break non-covalent bonds is in the pN range, and cells generally apply 10 to 1,000 fN of force per integrin [27, 28], with a 4 pN force being sufficient to disrupt nascent adhesion formation at the leading edge [29].

IV. Estimation of the force and time required to polarize protein distribution

To estimate the force required to skew the distribution of a membrane protein, we can consider a force, F_e, acting on a membrane protein that drifts with speed, v_p,

$$v_p = \frac{F_e}{\zeta}$$

where ζ is the drag coefficient. From the Einstein relationship,

$$\zeta = \frac{k_B T}{D_p}$$

where D_p is the diffusion constant of the protein and $k_B T$ is the thermal energy of the system. Over a given length scale for the development of asymmetry, L, (∼10 μm from the front to back of motile keratocyte), the protein distribution would be notably skewed if

$$v_p L > D_p$$

or,

$$F_e > \frac{k_B T}{L} \sim 0.4 \text{ fN} \tag{10}$$

Given that the net electric force will be roughly equivalent to the coulombic force, then

$$F_e = qE = ze^- E$$

where q is the effective charge of a protein with z elementary charges, e^-; then a given protein can achieve significant polarization in a 1 V/cm electric field with approximately 25 elemental charges. This is a number of charges that is certainly possible for a cluster of a few proteins, or even for a single protein, particularly one that is heavily glycosylated.

This redistribution of membrane proteins will occur on a time scale that is set by the drift speed of the protein, which is equivalent to the electrophoretic velocity, and is set by the both the strength of the electric field and the local viscosity as dictated by the Smoluchowski theory of electrophoresis, as long as the particle size is significantly larger than the Debye length. The resulting mobility of the proteins will be:

$$\mu_e = \frac{v}{E} = \frac{\varepsilon_r \varepsilon_0 \zeta}{\eta} \tag{11}$$

To more accurately assess the local viscosity, η, for a membrane component tethered to the membrane we must consider both the local drag forces exerted by the membrane as well as the extracellular fluid [12]. From the Saffman-Delbrük model, the drag force and consequently the mobility will be dependent on the viscosity of the aqueous environment of the cell [30], which will help dictate the rate of polarization of membrane components, and thus possibly the time for the cell to respond to an electric field. In addition once the electric field is turned off, the time for a cell to forget that it was in an electric field will be dependent on thermal diffusion alone and will also increase with increasing aqueous viscosity. This explicitly predicts that the *time to respond* will depend on the strength of the applied potential and aqueous viscosity. In addition, it should be noted that the *time to forget*, though primarily set by the aqueous viscosity, will also have some dependence on applied potential, due to greater polarization with higher field strengths, prior to turning the field off. We also found that, though the *time to switch* depends on cell size, the response strength does not. This could possibly be due to the cell determining directionality over a region of more fixed length, while still requiring a minimum threshold of polarization to this fixed region prior to activation.

The *time to forget* the effect of an electric field can be estimated as,

$$T_{forget} \sim L^2/D_p,$$

in this work we measured T_{forget} to be approximately 15 minutes or 10^3 seconds, thus we predict that $D_p \sim 0.1\ \mu m^2/sec$. This is about an order of magnitude slower than the diffusion coefficients measured for many integral

membrane proteins in pure lipid membranes, but is a realistic value for either the diffusion of a single protein in a membrane crowded by the presence of other proteins or for a protein that interacts with the cytoskeleton [31, 32].

In addition taking this value of the estimated D_p from the *time to forget* we can calculate an expected number of charges to produce the measured *time to respond*, $T_{respond}$. We know that the *time to respond* is proportional to the the length scale of the cell and the drift speed of the redistributed protein.

$$T_{respond} \sim L/v_p$$

Therefore, from above,

$$T_{respond} \sim \frac{Lk_bT}{ze^-ED_p}$$

or,

$$z \sim \frac{Lk_bT}{T_{respond}e^-ED_p} \tag{12}$$

Taking into account that $L \sim 10\mu m$, $k_BT \sim 0.004pN \times \mu m$, $T_{respond} \sim 300$ seconds, $e^- = 1.6 \times 10^{-19}C$, $E \sim 3V/cm = 3 \times 10^{14}pN/C$, and $D_p \sim 0.1\mu m^2/sec$ we can obtain an estimate of the number of elemental charges, $z \sim 25$. Remarkably, this is the same number of charges that we had estimated above as being the minimum required to produce significant polarization of charged membrane component, further supporting our conclusions that electrophoretic redistribution of membrane components is the signal guiding galvanotaxis. However, this does not take into a great deal of complexity including membrane protein trafficking within the cell and the non-spherical shape of the cell.

V. Modifying the salt concentration of media will alter the way electric fields interact with moving cells

In this work we have found that cells have a directional response that is proportional to the density of ionic current over the cell across a range of electric potentials and salt concentrations. We know that charged components of the membrane will feel both a coulombic force from the electric field and a drag force from electro-osmotic flow produced by ions at the cell membrane. Theoretically, then if ionic flow was the critical factor then it would reason that electro-osmotic flow is the essential force that cell's are responding to and not the applied potential directly. This, however, is an oversimplification. Changing the salt concentration will also change the zeta-potential of the membrane and the set of membrane components, as well as modify the thickness of the electrical double layer.

The thickness of the electrical double layer as discussed above scales with the inverse root of the ionic strength of the medium, thus lowering the salt concentration will increase the thickness of the double layer and should actually increase the speed of electro-osmotic fluid flow. Regarding the zeta potential, current literature on dilute solutions indicates that the zeta potential is expected to be proportional to the negative log of the ionic strength of solution and thus should be higher at low conductivity [33]. This would suggest that decreasing ion concentration would also increase the zeta potential and applied coulombic forces. However, these approximations are only valid in dilute solutions of electrolytes [34], which is quite unlike the highly charged surface of the cell. At the cellular surface there is no good theoretical understanding at this time of how the zeta potential will change with ionic strength. Given the results presented in this paper where the sensor for the electric field is electrophoresis of membrane components, and dependent on the zeta potential, we would expect that the zeta potential would decrease with decreasing ionic concentration. This has not been experimentally verified.

Supplemental Figures

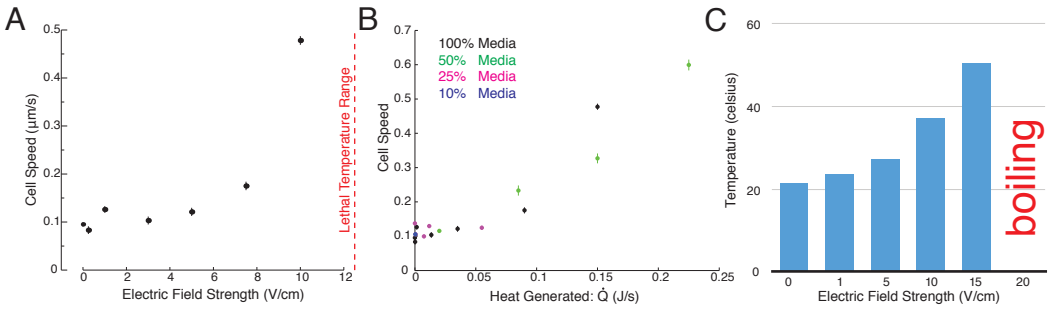

Figure S1. Elevated temperature drives the apparent electrokinetic behavior of keratocytes, Related to Figure 2

(a) The measured speed of populations of cells ± standard error at the given applied potentials. Cell speed increased with applied field strength, from 0.095 ± 0.003 μm/s without an electric field to 0.478 ± 0.009 μm/s in an electric field of 10 V/cm. Applied field strengths higher than 12.5 V/cm were lethal to cells, often after a very rapid re-orientation. However, we realized that an electric field will generate resistive heat ($\dot{Q}$) according to Joule's First Law

$$\dot{Q} \propto I^2 \times R = d \times I \times E \tag{13}$$

Where d is the length of the flow cell that the electric field was created across, and R is the resistance of the flow cell ($\sim 17,000$ Ω). This heat will be dissipated through the walls of the flow cell (180 μm on the bottom and 1000 μm on the top) as well as convective currents with the bulk media supply at the ends of the flow cell.

(b) When media salt concentrations, by dilution with water are changed (FBS concentration is kept fixed at 10%), cell speed is found to be a function of the heat produced ($\dot{Q}$) rather than current density or applied potential.

(c) Measured temperature in the flow cell was estimated from the decrease in fluorescence emission of Rhodamine B [35] at given applied potentials. Given that cell speed is a clear function of temperature [36], with a 2.3 fold increase in cell speed expected for every 10 degrees celsius increase in temperature (Allen et al. *in prep*), the change in cell speed is an expected result of the change in ambient temperature from joule heating. From this we can conclude that the electric field influences direction but not speed, and reports in the literature about speed increases in an electric field must be examined carefully for artifact.

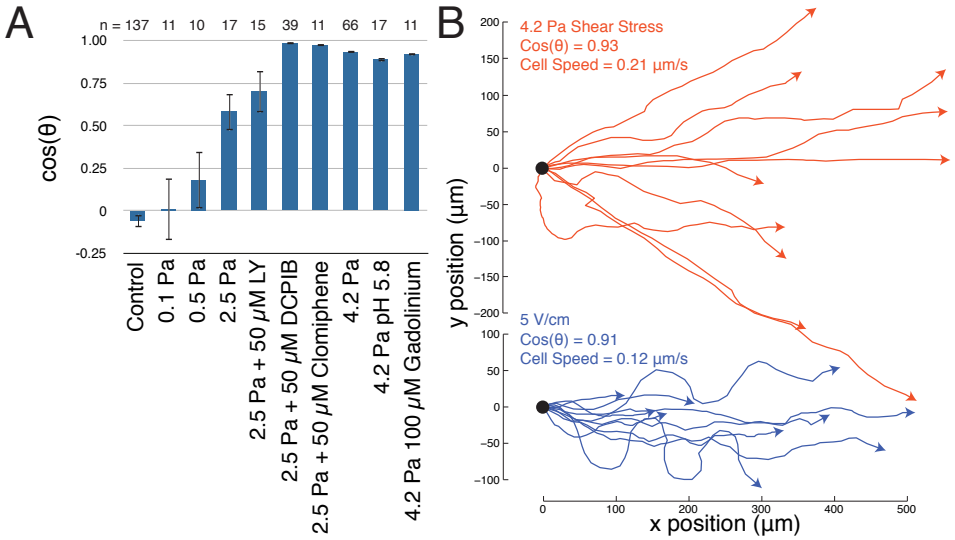

Figure S2. Keratocytes respond with directional migration to applied laminar fluid flow, Related to Figure 4

Cells exposed to laminar fluid flow were found to migrate in the direction of applied fluidic forces. (a) Calculated $\cos(\theta) \pm$ standard error for cells exposed to described shear stresses and perturbations. Perturbations include PI3K inhibitor LY-294002, volume regulated anion channel inhibitor DCPIB, PKC inhibitor clomiphene, an external pH of 5.8 and the stretch activated calcium channel inhibitor gadolinium. (b) Tracks of motile keratocytes under 4.2 Pa of shear stress from laminar flow (top, red), with fluid flow oriented to the right and cells exposed to an electric field of 5 V/cm (bottom, blue) with the cathode oriented toward the right.

Cells were observed to have slower speeds with long membrane protrusions when moving against the direction of flow and increased speeds with unusually small two-dimensional cell areas when moving in the direction of flow, which was not seen in galvanotaxis (**Movies S1,S2**). In addition, cells did not reorient completely parallel to the direction of flow, but instead frequently appeared to "tack", moving with surprising persistence at an oblique angle to the direction of flow. Again, this was not seen in cells undergoing galvanotaxis. The directional response was not dependent on intracellular signalling requiring the production of PIP3 or the activity of protein kinase C (PKC) as the PI3K inhibitor LY-294002 and the PKC inhibitor clomiphene failed to inhibit the directional response. This response was also insensitive to stretch activated calcium channel inhibitor gadolinium or volume regulated anion channel inhibitor, DCPIB.

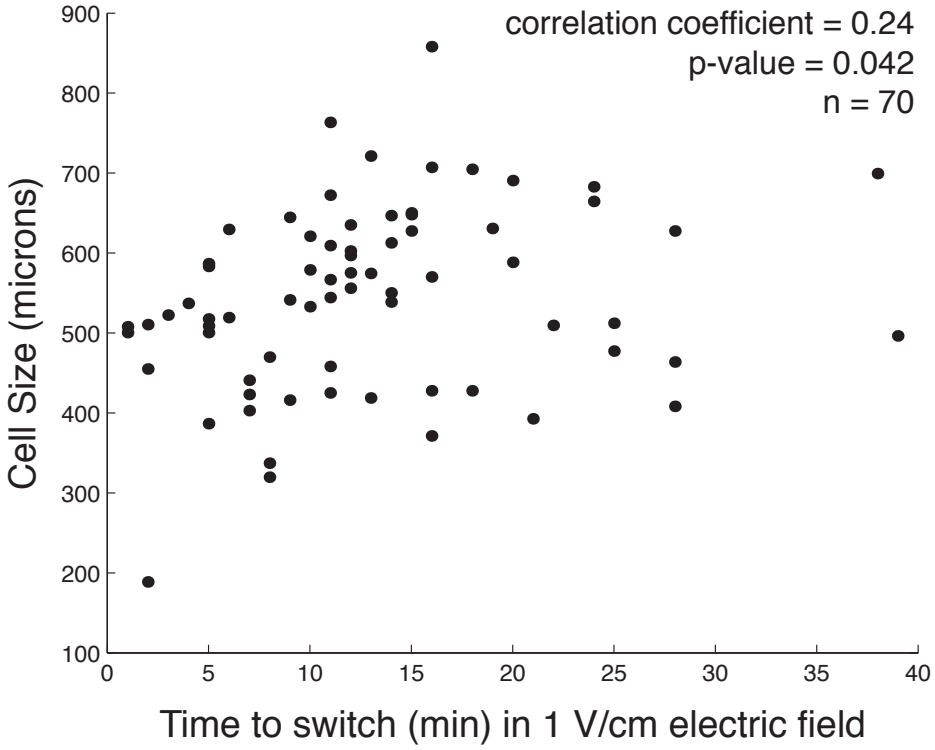

Figure S3. Time to switch directions in an electric field correlates with cell size, Related to Figure 6

The time for a cell to switch direction after the orientation of the cathode of a 1 V/cm electric field was reversed, was calculated for 70 individual cells and correlated to the size of the cell. A weak but statistically significant correlation was observed, with smaller cells re-orienting faster as would be expected if the kinetics of response depended on re-distribution of a membrane component.

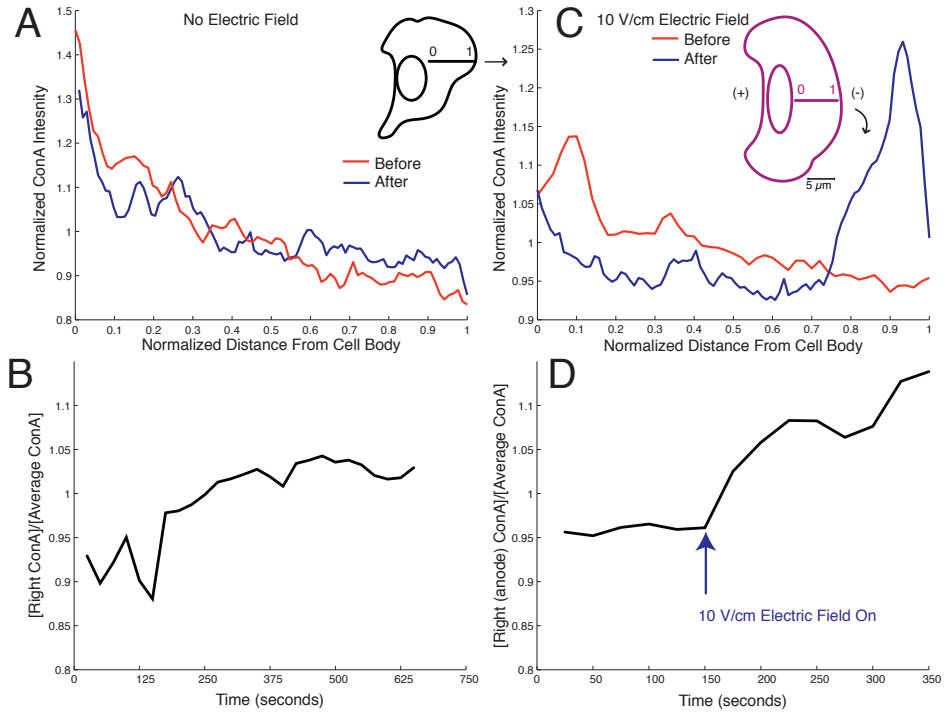

Figure S4. Fluorescent ConA redistributes to the anode in an electric field Related to Figure 6

The re-distribution of Texas Red labeled ConA was visualized in cells exposed to an electric field. (A) Measurement of the distribution of ConA from left to right in a control cell without an electric field at the start of the time lapse (red) and at the end of the time lapse (blue). (B) Time series of the relative intensity of ConA on the right side of the cell to the total ConA intensity for the control cell not in an electric field. There is no significant change in the distribution with time. (C) The same measurement was performed in a cell exposed to an electric field of 10 V/cm oriented with the cathode to the left. After exposure to the electric field there is a significant redistribution of ConA to the anodic (right) side. (D) The time series of the asymmetry in ConA distribution shows a rapid bias to the anode after exposure of the cell to an electric field. This is visualized in **Movie S4**.

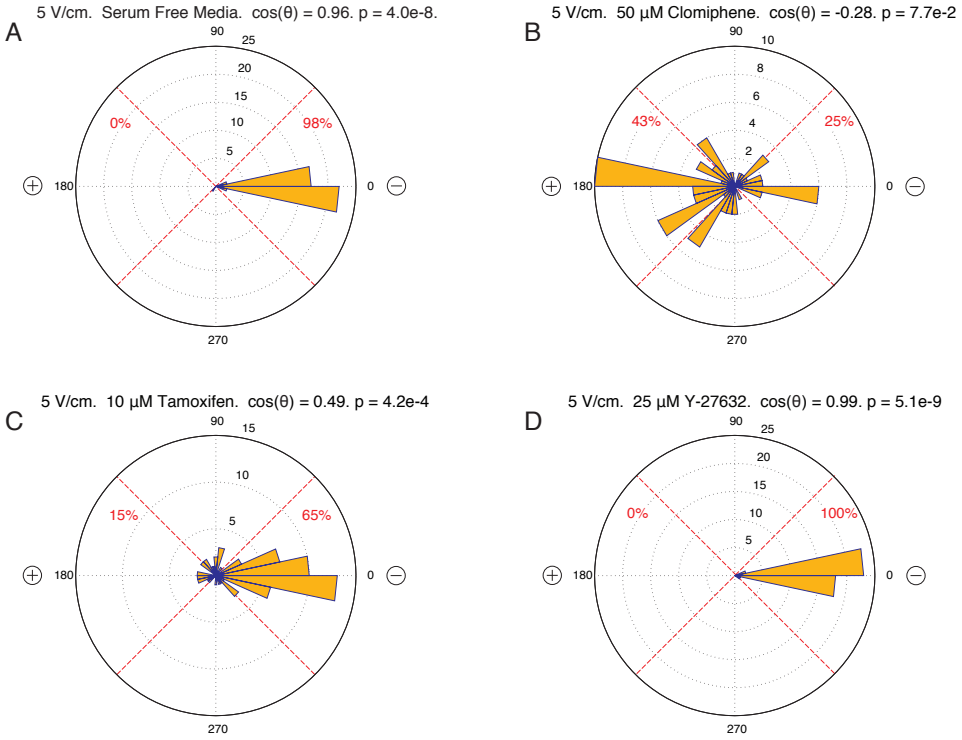

Figure S5. Inhibitors of signaling processes can inhibit galvanotaxis, Related to Figure 7

Rose plots of the trajectories of cells in (a) serum free media, (b) PKC inhibitor clomiphene, (c) PKC inhibitor tamoxifen, (d) Rho-associated kinase inhibitor Y-27632. The fraction of cells responding to the cathodic or anodic quartile are labeled in red. The p value is calculated from a Kolmogorov-Smirnov test for a uniform distribution of angles traveled. Serum free media and inhibition of Rho-associated kinase did not alter the galvanotactic response as compared to control cells at 5 V/cm as depicted in Figure 7. However, the PKC inhibitors clomiphene and tamoxifen had significant effects.

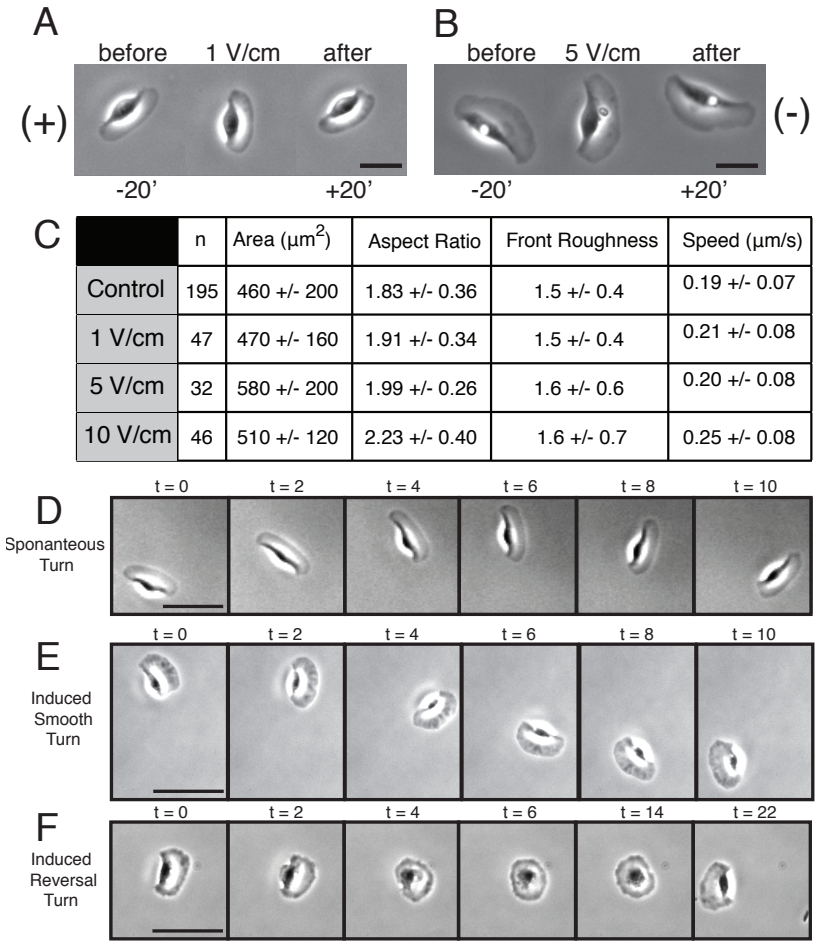

	n	Area (μm^2)	Aspect Ratio	Front Roughness	Speed (μm/s)
Control	195	460 +/- 200	1.83 +/- 0.36	1.5 +/- 0.4	0.19 +/- 0.07
1 V/cm	47	470 +/- 160	1.91 +/- 0.34	1.5 +/- 0.4	0.21 +/- 0.08
5 V/cm	32	580 +/- 200	1.99 +/- 0.26	1.6 +/- 0.6	0.20 +/- 0.08
10 V/cm	46	510 +/- 120	2.23 +/- 0.40	1.6 +/- 0.7	0.25 +/- 0.08

Figure S6. Keratocytes motile behavior is unchanged in an electric field, Related to Figure 2

Phase contrast images of cells imaged before application of an electric field, during the presence of an electric field, and after the electric field had been turned off for an electric field of 1 V/cm (a) and 5 V/cm (b). Cells were given > 10 minutes to equilibrate between each switch. Scale bars represent 50 microns. Cell shape is generally unchanged by the application of an electric field. (c) Quantitative descriptions of populations of cells imaged for 2 minutes each, at high spatial resolution (using high-numerical aperture oil immersion optics). Means +/- standard deviations are presented for each population. Front roughness is a measure of the local irregularity of the

leading edge, as described in Keren et al. (2008) [37].

Phase contrast images of three cells turning. (d) A cell turning spontaneously without the presence of electric field. (e,f) A cell turning under the directional cue of an electric field of 1 V/cm, with the cathode toward the left. The cell in e is representative of a cell undergoing a smooth turn and appears appreciably similar to a spontaneously turning cell. The cell in f is representative of a cell undergoing a reversal of direction with repolarization. Scale bar represents 50 microns. Time is represented as variable t, in minutes.

			(mA)			%		in um/s					
			mean	mean	var	cells		mean	var	mean	var		
	E-Field	Perturbation	I	cos(theta)	cos(theta)	forward	backward	speed	speed	Path Per	Path Per	p	n
Control	10 V/cm	none	3.0	**0.99**	0.00	100%	0%	**0.478**	0.009	0.961	0.005	1.03E-21	110
	7.5 V/cm	none	2.4	**0.99**	0.00	100%	0%	**0.175**	0.007	0.932	0.009	6.78E-18	89
	5 V/cm	none	1.4	**0.91**	0.09	94%	1%	**0.121**	0.005	0.891	0.014	5.86E-09	69
	3 V/cm	none	0.9	**0.97**	0.00	97%	0%	**0.103**	0.002	0.808	0.028	2.18E-05	29
	1 V/cm	none	0.3	**0.70**	0.26	77%	4%	**0.126**	0.010	0.677	0.391	4.42E-14	211
	1 V/cm	1% DMSO in SFM	0.4	**0.85**	0.10	84%	2%	**0.079**	0.001	0.688	0.027	2.58E-06	57
	0.25 V/cm	'0.25 V/cm'	0.1	**0.47**	0.33	48%	6%	**0.083**	0.002	0.646	0.079	3.11E-02	31
	0 V/cm	Control'	0.0	**-0.06**	0.45	22%	23%	**0.095**	0.003	0.664	0.079	0.56	137
Low Conductivity Media	15 V/cm	50% Media	3.0	**0.97**	0.01	97%	0%	**0.600**	0.018	0.948	0.011	8.89E-13	72
	12.5 V/cm	50% Media	2.4	**0.99**	0.00	100%	0%	**0.327**	0.010	0.929	0.006	2.43E-10	50
	10 V/cm	50% Media	1.7	**0.97**	0.01	98%	0%	**0.233**	0.010	0.895	0.020	8.18E-08	43
	10 V/cm	25% Media	1.1	**0.91**	0.07	91%	0%	**0.124**	0.001	0.810	0.027	1.66E-04	34
	5 V/cm	50% Media	0.8	**0.92**	0.02	92%	0%	**0.115**	0.002	0.833	0.029	1.60E-10	65
	5 V/cm	25% Media	0.5	**0.87**	0.10	89%	1%	**0.129**	0.003	0.937	0.004	4.30E-12	96
	5 V/cm	10% Media	0.3	**0.63**	0.33	66%	8%	**0.099**	0.001	0.820	0.029	2.51E-03	50
	1 V/cm	10% Media	0.0	**0.02**	0.51	27%	23%	**0.090**	0.001	0.547	0.049	0.46	295
	1 V/cm	25% Media	0.1	**0.42**	0.44	52%	12%	**0.105**	0.002	0.855	0.027	1.24E-04	142
	none	25% Media	0.0	**-0.05**	0.50	21%	31%	**0.137**	0.002	0.842	0.028	9.42E-03	137
Salt Free Solutions	5 V/cm	K+ Free HBSS	1.6	**0.97**	0.01	96%	0%	**0.110**	0.002	0.824	0.018	2.32E-14	90
	5 V/cm	Na+ Free, K+ enriched HBSS	1.9	**0.83**	0.18	88%	3%	**0.115**	0.004	0.782	0.038	4.15E-04	32
	5 V/cm	Na+ Free, Cs+ enriched HBSS	1.9	**0.86**	0.20	92%	6%	**0.130**	0.005	0.839	0.027	1.06E-08	52
	5 V/cm	10 uM Bapta-AM	1.4	**0.88**	0.10	88%	0%	**0.228**	0.003	0.827	0.055	3.57E-04	24
	1 V/cm	Na+ Free, K+ enriched HBSS	0.4	**0.57**	0.52	71%	14%	**0.055**	0.000	0.636	0.108	5.29E-02	7
Surface Charge	1 V/cm	20 ug/mL Poly-L-Lysine	0.3	**0.81**	0.13	80%	1%	**0.131**	0.002	0.702	0.040	7.57E-08	84
	1 V/cm	2 ug/mL Poly-L-Lysine	0.4	**0.74**	0.23	76%	4%	**0.166**	0.005	0.620	0.069	2.02E-04	51
Ion Channel Inhibitors	5 V/cm	25 uM Verapamil	1.6	**0.97**	0.04	99%	1%	**0.113**	0.006	0.888	0.015	1.52E-15	89
	5 V/cm	50 uM DCPIB	1.7	**1.00**	0.00	100%	0%	**0.138**	0.003	0.965	0.001	1.34E-16	81
	5 V/cm	50 uM Quinine	1.7	**0.98**	0.02	99%	0%	**0.133**	0.005	0.910	0.009	2.35E-19	107
	5 V/cm	10 uM Bafilomycin	1.5	**0.96**	0.01	98%	0%	**0.147**	0.002	0.849	0.037	5.86E-09	56
	5 V/cm	20 uM Amiloride	1.6	**0.98**	0.00	100%	0%	**0.075**	0.003	0.921	0.004	8.07E-10	56
	5 V/cm	10 mM ATP	1.6	**0.98**	0.01	99%	0%	**0.191**	0.005	0.898	0.020	9.20E-24	143
	5 V/cm	10 mM ADP	1.6	**0.93**	0.07	96%	0%	**0.169**	0.004	0.821	0.038	2.47E-09	51
	1 V/cm	25 uM DCPIB in SFM	0.4	**0.71**	0.14	65%	3%	**0.071**	0.000	0.650	0.054	4.86E-03	37
	1 V/cm	10 uM Bafilomycin in SFM	0.4	**0.47**	0.36	53%	13%	**0.048**	0.000	0.710	0.057	6.66E-02	30
Ionophores	5 V/cm	10 uM A-23187	1.6	**0.98**	0.00	100%	0%	**0.124**	0.005	0.834	0.027	5.50E-11	61
	5 V/cm	1 mM Dinitrophenol	1.4	**0.92**	0.06	96%	0%	**0.074**	0.000	0.814	0.046	2.47E-04	27
Signalling Pathway Inhibitors	5 V/cm	SFM	1.5	**0.96**	0.05	98%	0%	**0.168**	0.003	0.919	0.007	3.99E-08	44
	5 V/cm	50 uM LY-294002	1.4	**-0.41**	0.73	20%	70%	**0.082**	0.004	0.867	0.043	2.49E-03	81
	5 V/cm	10 uM Tamoxifen	1.5	**0.49**	0.52	65%	15%	**0.105**	0.003	0.710	0.067	4.24E-04	66
	5 V/cm	50 uM Clomiphene	1.7	**-0.28**	0.60	25%	43%	**0.193**	0.006	0.560	0.071	7.65E-02	65
	5 V/cm	25 uM Y-27632	1.4	**0.99**	0.00	100%	0%	**0.128**	0.002	0.914	0.012	5.09E-09	45
	1 V/cm	HBSS	0.4	**0.76**	0.22	72%	4%	**0.068**	0.001	0.691	0.050	2.67E-03	25
	1 V/cm	SFM	0.3	**0.51**	0.36	58%	10%	**0.123**	0.002	0.578	0.080	6.78E-03	31
	1 V/cm	50 uM LY-294002	0.3	**0.26**	0.65	47%	25%	**0.110**	0.003	0.760	0.074	0.21	32
	none	50 uM LY-294002	0.0	**-0.14**	0.42	20%	20%	**0.058**	0.001	0.706	0.074	0.74	15
Extracellular pH range	5 V/cm	pH 5.3 Citrate	1.5	**0.10**	0.52	33%	23%	**0.134**	0.003	0.494	0.055	0.57	83
	5 V/cm	pH 5.8 MES	1.8	**-0.12**	0.60	29%	35%	**0.138**	0.002	0.545	0.091	0.33	49
	5 V/cm	pH 6 MES	1.6	**0.46**	0.43	50%	9%	**0.135**	0.002	0.619	0.055	4.96E-02	22
	5 V/cm	pH 6.2 MES	1.7	**0.82**	0.09	76%	1%	**0.167**	0.002	0.791	0.035	1.86E-06	70
	5 V/cm	pH 6.8 HEPES	1.6	**0.83**	0.28	91%	9%	**0.185**	0.009	0.786	0.076	1.82E-04	23
	5 V/cm	pH 8 HEPES	1.7	**0.97**	0.00	96%	0%	**0.152**	0.004	0.893	0.013	7.45E-06	28
	5 V/cm	pH 8.5 Tris	1.1	**0.99**	0.00	100%	0%	**0.234**	0.003	0.974	0.002	2.27E-16	86
	5 V/cm	pH 9.5 Carbonate	1.5	**0.91**	0.04	88%	0%	**0.184**	0.004	0.879	0.026	1.64E-03	16
	1 V/cm	pH 5.8 MES	0.3	**0.33**	0.42	41%	9%	**0.126**	0.002	0.552	0.067	0.32	22
	1 V/cm	pH 6.2 MES	0.3	**0.62**	0.31	69%	7%	**0.158**	0.002	0.730	0.037	6.61E-03	29
	1 V/cm	pH 8.5 Tris	0.3	**0.64**	0.29	68%	4%	**0.231**	0.003	0.779	0.058	9.95E-04	56
	none	pH 6.0 MES	0.0	**0.00**	0.50	20%	33%	**0.122**	0.002	0.576	0.117	0.04	15
	none	pH 8.5 Tris	0.0	**0.01**	0.47	29%	22%	**0.198**	0.002	0.677	0.095	0.32	45
Cytoskeletal Inhibitors	10 V/cm	50 uM Blebbistatin	3.5	**0.98**	0.00	99%	0%	**0.453**	0.020	0.928	0.014	0.00	84
	5 V/cm	100 um Gadolinium	1.5	**0.91**	0.11	94%	3%	**0.128**	0.004	0.774	0.064	0.00	33
	5 V/cm	400 uM Soluble RGD	1.5	**0.98**	0.00	100%	0%	**0.053**	0.000	0.815	0.017	0.01	11
	5 V/cm	100 uM Blebbistatin	1.5	**0.98**	0.00	100%	0%	**0.272**	0.004	0.931	0.005	0.00	53
	5 V/cm	100 uM PF-228	1.6	**0.93**	0.01	94%	0%	**0.067**	0.001	0.895	0.006	0.00	35
	1 V/cm	50 uM Blebbistatin	0.4	**0.65**	0.28	70%	5%	**0.055**	0.000	0.670	0.057	0.07	20
	1 V/cm	20 uM Gadolinium	0.4	**0.88**	0.07	90%	0%	**0.075**	0.001	0.730	0.037	0.00	50
	1 V/cm	25 uM FAK-14	0.4	**0.87**	0.05	86%	0%	**0.082**	0.002	0.724	0.047	0.00	21
	Shear:												
Flow	0.1 Pa	Control	0	**-0.01**	0.61	18%	36%	**0.056**	0.001	0.622	0.089	0.89	11
	0.5 Pa	Control	0	**-0.18**	0.53	20%	30%	**0.084**	0.002	0.741	0.055	0.81	10
	2.5 Pa	Control	0	**0.58**	0.45	71%	6%	**0.130**	0.008	0.822	0.025	2.09E-02	17
	2.5 Pa	50 uM LY-294002	0	**0.70**	0.48	80%	13%	**0.133**	0.005	0.860	0.023	2.48E-03	15
	2.5 Pa	50 uM DCPIB	0	**0.98**	0.00	97%	0%	**0.136**	0.004	0.930	0.012	7.14E-07	39
	2.5 Pa	50 uM Clomiphene	0	**0.97**	0.00	100%	0%	**0.179**	0.001	0.959	0.001	2.77E-02	11
	4.2 Pa	Control	0	**0.93**	0.01	94%	0%	**0.212**	0.008	0.868	0.033	6.86E-14	66
	4.2 Pa	pH 5.8 MES	0	**0.89**	0.06	82%	0%	**0.131**	0.001	0.888	0.012	4.66E-03	17
	4.2 Pa	100 uM Gadolinium	0	**0.92**	0.03	82%	0%	**0.143**	0.002	0.944	0.003	4.12E-02	11

A-23187	Calcium Ion Ionophore
ADP	Acts as Anion Channel Inhibitor
Amiloride	Na-H exchanger (NHE1) and epithelial sodium channel (ENaC) inhibitor.
ATP	Acts as Anion Channel Inhibitor
Bafilomycin	Vacuolar-Type H+ ATPase inhibitor.
BAPTA-AM	Intracellular Calcium Chelator
Blebbistatin	Inhibits Non-Muscle Myosin II
Clomiphene	Inhibits Protein Kinase C
DCPIB	Volume Regulated Anion Channel (VRAC) inhibitor
Dinitrophenol	Hydrogen Ion Ionophore
FAK-14	Inhibits Focal Adhesion Maturation
Gadolinium	Gadolinium, Stretch Activated Calcium Channel Inhibitor
HBSS	Hanks Buffered Salt Solution
PF-228	Inhibits Focal Adhesion Maturation
Poly-L-Lysine	Positively charged homo-polymer that reverses bulk electro-osmotic flow
Quinine	Volume Regulated Anion Channel (VRAC) inhibitor
SFM	Liebowitz-15 Media with 1% ABAM but no FBS
Soluble RGD	Inhibits Integrin Binding
Staurosporine	Kinase inhibitor that promotes fragment formation.
Tamoxifen	Inhibits Protein Kinase C
Verapamil	L-Type Voltage Gated Ca++ Channel Inhibitor
Y-27632	Inhibits Rho Associated Protein Kinase

I:	Measured Current In Flow Cell in milliamps
Theta:	Angle Traveled by each cell.
Forward:	Cells that travel within +/- 45 degrees of the cathode
Backward:	Cells that travel within +/- 45 degrees of the anode.
Cell Speed	Measured from average of each cell displacament over 1 minute.
Path Per:	Net displacement divded by distance traveled.
P:	Probability of sampling from a uniform distribution of angles.
N:	Number of cells.

Figure S7. Partial data set, Related to Figures 2, 3, 4, 5, and 7

Summary of the most significant sets of population data of keratocytes exposed to various perturbations. Legend below lists perturbations, and defines table headers.

Supplemental Experimental Procedures

Cell Culture

Scales from the Central American cichlid *Hypsophys nicaraguensis* were isolated and cultured between two 18 mm coverslips with 23 μL of Leibowitz-15 media (Invitrogen) supplemented with 10% fetal bovine serum (Gemini Bio-Products) and 1% ABAM (Invitrogen) for one to three days. Cells were isolated with .25% Trypsin and replated on to a viewing surface, typically an Ibidi μ-slide I flowcell (Ibidi). Prior to replating, flow cells were washed with 0.1 % Triton-X 100 in 0.1 M NaOH, followed by 2 M solution of KCl in 1 M Tris at a pH of 7.4, then washed with acetone for ten minutes followed by a brief wash in isopropanol. Human red blood cells were isolated from a finger stick with an Autolet II (Owen Mumford) into 0.1 % EDTA in PBS, spun at 300 RPM for 30 seconds and then resuspended in Leibowitz-15 media.

Galvanotaxis

Cells were exposed to DC electric fields by replating cells into flow cells of minimal thickness and width to minimize Joule heating. Flexible Tygon tubing was filled with 2% agarose in Steinberg's Salt Solution [38], and used to connect the media on each side of the flow cell to a pair of salt water baths. Platinum electrodes ran out of the salt water baths and were connected to a regulated high voltage power supply (Schlumberger). Potential drop was measured in parallel across the flow cell, and current was measured in series with the constructed circuit using multimeters.

Measurement and control of pH

Intracellular pH was measured using the ratiometric excitation of BCECF (Santa-Cruz Biotech). Cells were loaded with 10 μM BCECF-AM for 15 minutes in serum free media. The ratio of emission at 535 nm following excitation at 440 nm versus 495 nm was measured using filter set 71001a (Chroma) to create a spatial map of any relative pH gradient. Culture pH was set by titrating Leibowitz-15 media with 10% fetal bovine serum with 15 mM of appropriate buffers. For media with a pH of 4.5 and 5.3, citrate buffer was used. For media with a pH of 5.8, 6.0, or 6.2, MES buffer was used. For media with a pH of 6.8, 7.4, or 8.0, HEPES buffer was used. For media with a pH of 8.5, Tris buffer was used. For media with a pH of 9.5, carbonate buffer was used.

Imaging

Cells were imaged at room temperature exposed to ambient atmosphere on either a Nikon Diaphot 300, a Nikon Eclipse TiE, or a Zeiss TIRF Axiovert. Transmitted light images were obtained using phase-contrast optics with both oil and air immersion objectives. Fluorescence images were taken with high numerical aperture oil immersion objectives using wide field illumination. Images were collected on 1k back-thinned EM-CCD cameras, Andor DU888 (Andor) or Hamamatsu ImageEM (Hamamatsu).

Cell tracks were reconstructed manually from cellular positions sampled at time resolution of 60 seconds and a typical spatial resolution of 0.56 μm/pixel. Perturbations were applied 15 minutes prior to onset of electric field (if present). The electric field was applied 15 minutes prior to imaging. Only tracks greater than 8 minutes in duration and with a mean speed greater than 0.035 μm/s were retained for analysis. The total data set acquired was 9,144 cell tracks over 201 different perturbations, (see **Figure S7** for a partial list). Path persistence was calculated for each track by the ratio of distance displaced to total distance traveled. Direction of travel (θ) was calculated with 0 degrees being toward the cathode and 180 degrees being towards the anode, such that a $cos(\theta) = 1$ indicates a completely cathodal trajectory, a $cos(\theta) = 0$ indicates no response and a $cos(\theta) = -1$ indicates a completely anodal trajectory. Path direction was calculated from the start point to the end point of each trajectory. For time of response experiments, direction at each time point was calculated from the time point t_i to the next time point t_{i+1}. Cell shape and size was determined by manual segmentation using the magnetic-lasso tool in Adobe Photoshop and analyzed with the freely available CellTool software suite [39].

Fluid flow

Electro-osmotic flow was measured by particle image velocimetry using 500 nm fluorescent microspheres (weakly charged such that electro-osmotic forces would dominate electro-static forces). Flow cells were coated by incubating unused tissue culture treated flow cells with 1 mg/mL poly-L-lysine for one hour to produce an expected surface density of 10 $\mu g/cm^2$. The flow cell was then filled with a solution of 0.5 nM COOH-YG beads (Polysciences) and a electric field through the flow cell was created as discussed above. Bead motion was measured as a stream acquisition using wide field fluorescence on a 60x (1.4 NA) objective at different focal planes throughout the bottom half of the flow cell. The top half of the flow cell was assumed to show symmetrical flow.

Laminar fluid flow was created by replating cells into a flow cell with luer lock connectors at each end, μ-slide I luer (Ibidi). Luer connections to a FPLC pump, Pharmacia P500 (Pharmacia), were made and the pump was run at a set volumetric flow rate. Shear stress in the flow cell was calculated based on the dynamic viscosity of $\zeta = 0.01\ dyn * s/cm^2$ per the flow cell manufacturer's specifications. Flow rates of 0.19 mL/min, 0.97 mL/min, 4.87 mL/min and 8.33 mL/min produced shear stresses of 0.1, 0.5, 2.5, and 4.25 Pa respectively.

Electrophoretic mobility

The elelctrophoretic mobility of cells can be determined by the motion of suspended cells in an electric field. Given an expected charge density in the tens of millions per cell, electrophoretic forces should exceed drag from bulk electro-osmotic flow (< 10 μm/s) by at least three orders of magnitude. Keratocyte cells were stained with 50 μM calcein-AM (BD) and imaged with 500 nm YG-beads (Polysciences) present as a control for bulk electro-osmotic flow. Cells were placed in a $\sim$800 μm tall flow cell coated with 100 μg/mL poly-L-lysine-PEG and imaged immediately to inhibit cell adhesion. Electric fields were applied as described above and cell motion was measured by a stream acquisition using an air objective and wide-field fluorescence excitation for keratocytes and phase-imaging for red blood cells.

ConA distribution

The distribution of ConA was measured following incubation of cells with 100 μmg/mL Texas Red conjugated Concavalin A (Molecular Probes) for 15 minutes, followed by washing with media. Live stained cells were then imaged with high numerical aperture oil immersion optics using wide-field fluorescence.

Pharmacological Inhibitors

Pharmacological inhibitors were used at or above previously determined optimal concentrations of 25 μM verapamil (Sigma) [40], 50 μM DCPIB (Sigma) [41], 50 μM quinine (Sigma) [42], 10 μM A-23187 (Sigma) [43], 10 μM bafilomycin (Santa Cruz Biotechnology) [44], 10-100 μM gadolinium (Aldrich) [7], 25 μM Y-27632 (Calbiochem) [45] and 100 μM (-)-blebbistatin (Fischer Scientific) [46]. Alternatively inhibitors were used at empirically determined maximal tolerable concentrations for 20 μM amiloride hydrochloride (Sigma), 50 μM LY-294002 (Calbiochem), 10 μM tamoxifen (Sigma), 100 μM PF-573228 (Tocris), and 25 μM FAK inhibitor 14 (Tocris).

Temperature Measurement

Temperature in the flow cell was approximated using the intensity of rhodamine B fluorescence [35]. Using a solution of 67 μM rhodamine B in Leibowitz-15 Media + 10% FBS with temperature set by a hot-water bath and measured by a thermocouple, a control curve of fluorescence intensity was determined and fit by linear regression between 22.5 and 48° C. The experimental temperature was then interpolated from this control curve by measurement of the fluorescence intensity under identical imaging conditions following application of an external electric field for 10 minutes.

Supplemental References

[1] D. Lee, W. Grill, Polarization of a spherical cell in a nonuniform extracellular electric field, Annals of Biomedical Engineering 33 (5) (2005) 603–615. doi:DOI 10.1007/s10439-005-2397-3.

[2] R. Phillips, J. Kondev, J. Theriot, Physical Biology of the Cell, Garland Science, 2009.

[3] A. L. Hodgkin, A. F. Huxley, A quantitative description of membrane current and its application to conduction and excitation in nerve, J Physiol 117 (4) (1952) 500–44.

[4] Z. Lojewska, D. L. Farkas, B. Ehrenberg, L. M. Loew, Analysis of the effect of medium and membrane conductance on the amplitude and kinetics of membrane potentials induced by externally applied electric fields, Biophys J 56 (1) (1989) 121–8. doi:10.1016/S0006-3495(89)82657-8.

[5] B. J. Mossop, R. C. Barr, D. A. Zaharoff, F. Yuan, Electric fields within cells as a function of membrane resistivity–a model study, IEEE Trans Nanobioscience 3 (3) (2004) 225–31.

[6] Y.-H. Sun, M. Zhao, A. Mogilner, Keratocyte fragments and cells utilize competing pathways to move in opposite directions in electric field, Current Biology.

[7] L. Huang, P. Cormie, M. A. Messerli, K. R. Robinson, The involvement of Ca2+ and integrins in directional responses of zebrafish keratocytes to electric fields, J Cell Physiol 219 (1) (2009) 162–72. doi:10.1002/jcp.21660.

[8] W. D. Stein, Channels, Carriers and Pumps: An Introduction to Membrane Transport, Academic Press, 1990.

[9] B. S. Pallotta, K. L. Magleby, J. N. Barrett, Single channel recordings of Ca2+-activated K+ currents in rat muscle cell culture, Nature 293 (5832) (1981) 471–4.

[10] N. Minc, F. Chang, Electrical control of cell polarization in the fission yeast Schizosaccharomyces pombe, Curr Bioldoi:10.1016/j.cub.2010.02.047.

[11] L. Kjellén, U. Lindahl, Proteoglycans: structures and interactions, Annu Rev Biochem 60 (1991) 443–75. doi:10.1146/annurev.bi.60.070191.002303.

[12] C. Yoshina-Ishii, S. G. Boxer, Controlling two-dimensional tethered vesicle motion using an electric field: interplay of electrophoresis and electro-osmosis, Langmuir 22 (5) (2006) 2384–91. doi:10.1021/la0526277.

[13] H. Stone, A. Stroock, A. Ajdari, Engineering flows in small devices: Microfluidics toward a lab-on-a-chip, Annual Review of Fluid Mechanics 36 (2004) 381–411. doi:DOI 10.1146/annurev.fluid.36.050802.122124.

[14] S.-S. Hsieh, H.-C. Lin, C.-Y. Lin, Electroosmotic flow velocity measurements in a square microchannel, Colloid and Polymer Science 284 (11) (2006) 1275–1286. doi:DOI 10.1007/s00396-006-1508-5.

[15] P. Stevenson, R. Thorpe, J. Davidson, Incipient motion of a small particle in the viscous boundary layer at a pipe wall, Chemical Engineering Science 57 (21) (2002) 4505–4520.

[16] C. A. Brunner, A. Ehrlicher, B. Kohlstrunk, D. Knebel, J. A. Käs, M. Goegler, Cell migration through small gaps, Eur Biophys J 35 (8) (2006) 713–9. doi:10.1007/s00249-006-0079-1.

[17] A. B. Verkhovsky, T. M. Svitkina, G. G. Borisy, Self-polarization and directional motility of cytoplasm, Curr Biol 9 (1) (1999) 11–20.

[18] C. P. Cheng, D. Parker, C. A. Taylor, Quantification of wall shear stress in large blood vessels using lagrangian interpolation functions with cine phase-contrast magnetic resonance imaging, Ann Biomed Eng 30 (8) (2002) 1020–32.

[19] S. Noria, F. Xu, S. McCue, M. Jones, A. I. Gotlieb, B. L. Langille, Assembly and reorientation of stress fibers drives morphological changes

to endothelial cells exposed to shear stress, Am J Pathol 164 (4) (2004) 1211–23. doi:10.1016/S0002-9440(10)63209-9.

[20] E. Décave, D. Rieu, J. Dalous, S. Fache, Y. Brechet, B. Fourcade, M. Satre, F. Bruckert, Shear flow-induced motility of dictyostelium discoideum cells on solid substrate, J Cell Sci 116 (Pt 21) (2003) 4331–43. doi:10.1242/jcs.00726.

[21] A. I. Barakat, A model for shear stress-induced deformation of a flow sensor on the surface of vascular endothelial cells, J Theor Biol 210 (2) (2001) 221–36. doi:10.1006/jtbi.2001.2290.

[22] N. Ofer, A. Mogilner, K. Keren, Actin disassembly clock determines shape and speed of lamellipodial fragments, Proc Natl Acad Sci U S A 108 (51) (2011) 20394–9. doi:10.1073/pnas.1105333108.

[23] K. M. Lipman, R. Dodelson, R. M. Hays, The surface charge of isolated toad bladder epithelial cells. Mobility, effect of pH and divalent ions, J Gen Physiol 49 (3) (1966) 501–16.

[24] R. Phillips, T. Ursell, P. Wiggins, P. Sens, Emerging roles for lipids in shaping membrane-protein function, Nature 459 (7245) (2009) 379–85. doi:10.1038/nature08147.

[25] K. I. Anderson, R. Cross, Contact dynamics during keratocyte motility, Curr Biol 10 (5) (2000) 253–60.

[26] P. Kanchanawong, G. Shtengel, A. M. Pasapera, E. B. Ramko, M. W. Davidson, H. F. Hess, C. M. Waterman, Nanoscale architecture of integrin-based cell adhesions, Nature 468 (7323) (2010) 580–4. doi:10.1038/nature09621.

[27] L. Y. Koo, D. J. Irvine, A. M. Mayes, D. A. Lauffenburger, L. G. Griffith, Co-regulation of cell adhesion by nanoscale RGD organization and mechanical stimulus, J Cell Sci 115 (Pt 7) (2002) 1423–33.

[28] S. W. Moore, P. Roca-Cusachs, M. P. Sheetz, Stretchy proteins on stretchy substrates: the important elements of integrin-mediated rigidity sensing, Dev Cell 19 (2) (2010) 194–206. doi:10.1016/j.devcel.2010.07.018.

[29] S. Bohnet, R. Ananthakrishnan, A. Mogilner, J.-J. Meister, A. B. Verkhovsky, Weak force stalls protrusion at the leading

edge of the lamellipodium, Biophys J 90 (5) (2006) 1810–20. doi:10.1529/biophysj.105.064600.

[30] P. G. Saffman, M. Delbrück, Brownian motion in biological membranes, Proc Natl Acad Sci U S A 72 (8) (1975) 3111–3.

[31] F. Zhang, B. Crise, B. Su, Y. Hou, J. K. Rose, A. Bothwell, K. Jacobson, The lateral mobility of some membrane proteins is determined by their ectodomains, Biophys J 62 (1) (1992) 92–4. doi:10.1016/S0006-3495(92)81789-7.

[32] A. Kusumi, Y. Sako, M. Yamamoto, Confined lateral diffusion of membrane receptors as studied by single particle tracking (nanovid microscopy). Effects of calcium-induced differentiation in cultured epithelial cells, Biophys J 65 (5) (1993) 2021–40. doi:10.1016/S0006-3495(93)81253-0.

[33] B. Kirby, E. Hasselbrink, Zeta potential of microfluidic substrates: 1. Theory, experimental techniques, and effects on separations, Electrophoresis 25 (2) (2004) 187–202. doi:DOI 10.1002/elps.200305754.

[34] V. G. Levich, Physicochemical hydrodynamics, Prentice-Hall, Englewood Cliffs, N.J., 1962.

[35] J. J. Shah, M. Gaitan, J. Geist, Generalized temperature measurement equations for Rhodamine B dye solution and its application to microfluidics, Anal Chem 81 (19) (2009) 8260–3. doi:10.1021/ac901644w.

[36] R. A. Ream, J. A. Theriot, G. N. Somero, Influences of thermal acclimation and acute temperature change on the motility of epithelial wound-healing cells (keratocytes) of tropical, temperate and antarctic fish, J Exp Biol 206 (Pt 24) (2003) 4539–51.

[37] K. Keren, Z. Pincus, G. M. Allen, E. L. Barnhart, G. Marriott, A. Mogilner, J. A. Theriot, Mechanism of shape determination in motile cells, Nature 453 (7194) (2008) 475–80. doi:10.1038/nature06952.

[38] B. Song, Y. Gu, J. Pu, B. Reid, Z. Zhao, M. Zhao, Application of direct current electric fields to cells and tissues in vitro and modulation of wound electric field in vivo, Nat Protoc 2 (6) (2007) 1479–89. doi:10.1038/nprot.2007.205.

[39] Z. Pincus, J. A. Theriot, Comparison of quantitative methods for cell-shape analysis, J Microsc 227 (Pt 2) (2007) 140–56. doi:10.1111/j.1365-2818.2007.01799.x.

[40] M. Cooper, M. Schliwa, Motility of cultured fish epidermal-cells in the presence and absence of direct-current electric-fields, Journal of Cell Biology 102 (4) (1986) 1384–1399.

[41] N. Decher, H. J. Lang, B. Nilius, A. Brüggemann, A. E. Busch, K. Steinmeyer, DCPIB is a novel selective blocker of ICl,swell and prevents swelling-induced shortening of guinea-pig atrial action potential duration, British Journal of Pharmacology 134 (7) (2001) 1467–1479. doi:10.1038/sj.bjp.0704413.
URL http://dx.doi.org/10.1038/sj.bjp.0704413

[42] T. Voets, G. Droogmans, B. Nilius, Potent block of volume-activated chloride currents in endothelial cells by the uncharged form of quinine and quinidine., Br J Pharmacol 118 (7) (1996) 1869–1871.

[43] M. S. Cooper, M. Schliwa, Transmembrane Ca2+ fluxes in the forward and reversed galvanotaxis of fish epidermal cells, Prog Clin Biol Res 210 (1986) 311–8.

[44] E. J. Bowman, A. Siebers, K. Altendorf, Bafilomycins: a class of inhibitors of membrane ATPases from microorganisms, animal cells, and plant cells., Proc Natl Acad Sci U S A 85 (21) (1988) 7972–7976.

[45] P. T. Yam, C. A. Wilson, L. Ji, B. Hebert, E. L. Barnhart, N. A. Dye, P. W. Wiseman, G. Danuser, J. A. Theriot, Actin-myosin network reorganization breaks symmetry at the cell rear to spontaneously initiate polarized cell motility, J Cell Biol 178 (7) (2007) 1207–21. doi:10.1083/jcb.200706012.

[46] C. A. Wilson, M. A. Tsuchida, G. M. Allen, E. L. Barnhart, K. T. Applegate, P. T. Yam, L. Ji, K. Keren, G. Danuser, J. A. Theriot, Myosin II contributes to cell-scale actin network treadmilling through network disassembly, Nature 465 (7296) (2010) 373–7. doi:10.1038/nature08994.